Physics – Uspekhi **41** (5) 419 – 439 (1998)

REVIEWS OF TOPICAL PROBLEMS PACS numbers: 12.39.Mk, **12.38.–t**, **14.40.–n**

The lightest scalar glueball

V V Anisovich

Contents

Abstract. Recent studies of meson spectra have enabled the resonance structure of the $IJ^{PC} = 00^{++}$, 10^{++}, 02^{++}, 12^{++}, and $IJ^{P} = \frac{1}{2}0^{+}$ waves to be found for masses ranging up to 1900 MeV, thus fully reconstructing the $1^3P_0q\bar{q}$ and $2^3P_0q\bar{q}$ meson multiplets. There is firm experimental evidence for the existence of five scalar – isoscalar states in this mass range, four of which are $q\bar{q}$ states and members of the $1^3P_0q\bar{q}$ and $2^3P_0q\bar{q}$ nonets, whereas the fifth falls out of the quark picture and displays all the properties of the lightest possible scalar glueball. A dispersion analysis of the 00^{++} wave elucidates how the mixture of the pure glueball state (or gluonium) with neighboring scalar $q\bar{q}$ states forms: three scalar mesons, namely two relatively narrow $f_0(1300)$ and $f_0(1500)$ resonances and a very broad $f_0(1530^{+90}_{-250})$ resonance, share the gluonium, the broad resonance being the gluonium's descendant and accounting for about 40 to 50% of it.

To the memory of Yuriĭ Dmitrievich Prokoshkin

1. Introduction: retrospective view and the current state of the problem

A great variety of the currently observed mesons and baryons represent systems built of quarks: baryons, which are three-quark systems (qqq), and mesons, which are quark – antiquark bound states ($q\bar{q}$). More than 20 years ago the problem arose [1] of whether additional hadrons exist which are built out of another fundamental QCD particle, the gluon. An intensive search for the glueball — a particle consisting of gluons — has been carried out throughout these decades.

The first evaluation of glueball masses for different J^{PC} was done in the bag model [2]. According to this, the lightest glueballs are scalars and tensors, 0^{++} and 2^{++}; then follow pseudoscalar and pseudotensor glueballs, 0^{-+} and 2^{-+}.

Recently considerable progress has been achieved in lattice QCD calculations. The UKQCD Collaboration [3] obtained the following mass values for the lightest gluodynamical glueballs (i.e. glueballs without quark degrees of freedom taken into account):

$$m_G(0^{++}) = 1549 \pm 53\,\text{MeV}, \quad m_G(2^{++}) = 2310 \pm 110\,\text{MeV},$$
$$m_G(0^{-+}) = 2332 \pm 264\,\text{MeV}. \qquad (1.1)$$

Systematic errors are not included into the values given in Eqns (1.1); they are of the order of 100 MeV.

The IBM group obtained a slightly different value for the mass of the lightest scalar glueball [4]:

$$m_G(0^{++}) = 1740 \pm 71\,\text{MeV}. \qquad (1.2)$$

The result of Ref. [5] is as follows:

$$m_G(0^{++}) = 1630 \pm 60 \pm 80\,\text{MeV},$$
$$m_G(2^{++}) = 2400 \pm 10 \pm 120\,\text{MeV}. \qquad (1.3)$$

V V Anisovich St. Petersburg Nuclear Physics Institute
188350 Gatchina, St. Petersburg, Russia
Fax (7-812) 713 19 63
E-mail: anisovic@thd.pnpi.spb.ru

Received 4 November 1997
Uspekhi Fizicheskikh Nauk **168** (5) 481 – 502 (1998)
Submitted in English by the author; edited by L V Semenova

However, in the lattice calculations cited above the quark degrees of freedom have not been taken into account, since the existing computing facilities did not allow it. Quark degrees of freedom may significantly shift the position of the glueball mass. The dispersion relation analysis of meson spectra [6, 7], based on a restoration of the propagator matrix for scalar–isoscalar resonances, shows that mixing with $q\bar{q}$ states results in a mass shift of the order of 100 – 300 MeV. It should be stressed that, according to the $1/N$-expansion rules [8] ($N = N_f = N_c$, where N_f and N_c stand for the light flavor and color numbers), the mixing of a glueball with $q\bar{q}$ states is not suppressed.

Experimental searches for the glueballs have been particularly intensive over the last decade. There exist reactions where one could expect an enhanced production of glueballs. Central hadron production at the high-energy hadron – hadron collisions provides us with an example of such a reaction, because the particles in the central region are produced in the transition *pomerons* → *hadrons*. The pomeron is a gluon-rich system, so one could expect to find dominant production of glueballs among secondary hadrons, while the production of $q\bar{q}$ states is expected to be small. However, the data on central hadron production, with statistics sufficient to perform a reliable partial wave analysis, are only now appearing. More accessible for experimental study appeared to be another reaction, which is governed by the transition *gluons* → *hadrons*, i.e. radiative decays $J/\psi \to \gamma + hadrons$. In these decays, hadrons are formed by gluons created in $c\bar{c}$ annihilation; therefore one may expect dominant production of glueballs in this reaction. The experimental study of hadron spectra in radiative J/ψ decays has been carried out for 2 decades, and is still going on. Experimental information accumulated at the beginning of the 90's seemed to be rather discouraging: in radiative J/ψ decays $q\bar{q}$ states have been strongly produced. Meson production branching ratios presented in the Particle Data Group compilation [9] show a number of resonances produced with similar probabilities, such as η, η', $f_2(1270)$, $f_2(1525)$, etc., which certainly are $q\bar{q}$-dominant systems. Such a situation presents a dilemma:

(1) the glueball does not exist; it is 'an unfulfilled promise of QCD' [10];

(2) glueball states are mixed strongly with the $q\bar{q}$ mesons, so in experiments one observes just these mixed states.

Analysis of the 0^{++} wave [6, 7] definitely supports the second scenario.

Experimental data on the transition formfactors $\gamma\gamma^*(Q^2) \to \pi^0, \eta, \eta'$ [11] provide the following restrictions for probabilities of finding the glueball components in η and η' mesons: $W_\eta \leqslant 8\,\%$, $W_{\eta'} \leqslant 20\%$ [12]. This means that in the $q\bar{q}$ mesons observed in radiative J/ψ decay one could find a glueball component at the level of 5 – 10%. Hence, the admixture of the $q\bar{q}$ component in the glueball should be considerably more, since the glueball can mix with several $q\bar{q}$ mesons. This qualitative estimate agrees with that obtained in the framework of the $1/N$ expansion: according to this, the glueball component in each $q\bar{q}$ meson is of the order of $1/N_c$, while the $q\bar{q}$ component in the glueball is of the order of N_f/N_c [13]. Of course, it should be stressed that some specific cases may differ from this general evaluation, because the mixing depends strongly on the relative spacing of mixed levels.

If scenario (2) with strong mixing of the glueball and $q\bar{q}$ states is realized in nature, the search for the glueball is a laborious and difficult task involving the identification of mesons and their systematics. Naive expectations, such as a study of gluon-rich $\gamma\gamma$ reactions with the purpose of seeing direct glueball production cannot be expected to succeed.

The main channel of radiative J/ψ decays, as deduced from experimental data, is the production of broad hadron clusters. The production of these clusters may be viewed as a direct signal of strong mixing between the glueball and $q\bar{q}$ mesons. What happens is that, through mixing, one resonance accumulates the widths of other resonances. This effect was first observed in Ref. [14], where the low-energy part of the spectrum of the 0^{++} wave was analysed, and it was investigated in detail in Refs [6, 7]. When the two resonances mix completely with each other, one of them gets almost the whole width $\Gamma_1 + \Gamma_2$, while the width of the other tends to zero. In the case of an 'ideal' mixing of three resonances, the width of one of them accumulates the widths of the other two, $\Gamma_1 + \Gamma_2 + \Gamma_3$, and the widths of the others tend to zero. In reality, when the scalar glueball mixes with neighboring states, a qualitatively similar effect occurs; that is, a glueball situated among the scalar $q\bar{q}$ states mixes with them and accumulates a considerable part of their widths. From this point of view, the appearance of a broad resonance which is the glueball descendant is an inevitable consequence of the mixing. The broad resonance must be a neighbor of comparatively narrow resonances, which are the descendants of pure $q\bar{q}$ states; the broad resonance contains a considerable glueball admixture. The analysis of the 0^{++} wave in the mass range 1200 – 1800 MeV [6, 7], based on the dispersion relation representation, reconstructs just this picture of the lightest scalar glueball mixing with $q\bar{q}$ members of multiplets 1^3P_0 and 2^3P_0. One may predict that such a scenario of mixing is common for all low-lying glueballs.

Thus, the strong mixing of $q\bar{q}$ states with a gluonium does not allow easy identification of the glueball. In this case the only reasonable strategy is to study the systematics of all resonances in terms of $q\bar{q}$ multiplets. The extra states which do not fit into the systematics should be regarded as candidates for the glueballs or other exotic mesons. This investigation program has been declared in Ref. [13], and at the same time the first steps have been made in carrying it out: in Ref. [14] the K-matrix analysis has been performed for the low-energy part of the wave $IJ^{PC} = 0^{++}$.

Detailed analysis of meson states in the region 1000 – 2000 MeV was possible due to the huge amount of experimental data collected in the last decade by Crystal Barrel and GAMS Collaborations. The Crystal Barrel Collaboration has high-precision data on the production of three neutral mesons in the $p\bar{p}$-annihilation reaction at rest,

$$p\bar{p}\ (at\ rest) \to \pi^0\pi^0\pi^0\,, \quad \pi^0\pi^0\eta\,, \quad \pi^0\eta\eta\,, \tag{1.4}$$

with event numbers of 1500000 for $(\pi^0\pi^0\pi^0)$, 280000 for $(\pi^0\pi^0\eta)$ and 185000 for $(\pi^0\eta\eta)$. The data on the reaction $p\bar{p}\ (at\ rest) \to \pi^0\pi^0\pi^0$ with somewhat lower statistics were published in 1991 [15]. However, the first fits of the spectra did not provide a correct identification of scalar resonances, for certain special features of the three-particle decay were not taken into account. A critical analysis of the situation has been made in Refs [16, 17], where it was shown that a resonance near 1500 MeV, which had earlier been identified as a tensor one, $AX_2(1520)$, is actually a scalar resonance. Reanalysis of the reactions (1.4) within the T-matrix formalism

performed together with the Crystal Barrel Collaboration has confirmed the existence of new scalar resonances: $f_0(1500)$ [18] and $a_0(1450)$ [19]. In addition, in Refs [16–18] a significant production of the resonance $f_0(1360)$, with a half-width equal to 130 MeV, was identified, although at that time it was not quite clear whether this was a newly observed resonance or a fragment of the broad resonance $\epsilon(1300)$, widely discussed over the last decades. Later on, after having performed the *K*-matrix analysis for larger samples of data, it became clear that in this mass region there are two resonances — a comparatively narrow one, $f_0(1300)$, and a rather broad one, $f_0(1530^{+90}_{-250})$.

In the first stage of the investigation, the data fitting was done in the framework of the *T*-matrix technique. The reason was obvious: the *T*-matrix representation of the amplitude is simpler for data fitting; the advantages of the *K*-matrix approach reveal themselves only when information exists for all possible channels of the reaction. In the mass region 1000–1500 MeV, there are the following channels in the 0^{++} wave: $\pi\pi$, $K\bar{K}$, $\eta\eta$, and $\pi\pi\pi\pi$, while in the region above 1500 MeV the channel $\eta\eta'$ becomes also important. It was obvious that the application of the sophisticated *K*-matrix technique for fitting to a limited number of channels (1.4) would lead to some ambiguities.

The discovery of the resonance $f_0(1500)$ immediately gave rise to hypotheses of a close relation to the lightest scalar glueball, and the possibility of such a relation was stressed in Refs [17, 18]. In papers [13, 20–23], several schemes were suggested for the mixing of the lightest scalar glueball with the neighboring $q\bar{q}$ states. However, none of these schemes took account of the special features of the mixing which are due to the transition of a resonance into real mesons, although these very transitions, as was shown in a specified *K*-matrix analysis, determine the structure of the 0^{++} wave around 1500 MeV.

At the next stage of the 0^{++}-wave analysis, the GAMS data on the spectra $\pi^0\pi^0$, $\eta\eta$, and $\eta\eta'$ were included; these were obtained in the reactions [24–26]

$$\pi^- p \to n\pi^0\pi^0\,, \quad n\eta\eta\,, \quad n\eta\eta' \tag{1.5}$$

together with the data of the CERN–Münich Collaboration [27]:

$$\pi^- p \to n\pi^+\pi^- \tag{1.6}$$

and BNL [28] group:

$$\pi\pi \to K\bar{K}\,. \tag{1.7}$$

Simultaneous analysis of the whole data sample (1.4)–(1.7) was carried out in Refs [14, 29, 30] in the framework of the *K*-matrix technique; in this way the range of masses under investigation and the number of channels covered by the *K*-matrix fit of the 0^{++} amplitude gradually increased.

The first investigation [14] was done in the region of invariant meson energies $\sqrt{s} \leqslant 1100$ MeV for two channels only, namely, $\pi\pi$ and $K\bar{K}$. In this analysis an observation was made, which became later important: the transitions which are responsible for the decay of meson states are also responsible for a strong mixing of these states. Moreover, the masses of mixed states differ essentially from the primary ones. These 'primary mesons' were called 'bare mesons' [14], in contrast to physical states, for which the cloud of real particles, $\pi\pi$ and $K\bar{K}$, plays an important role in their formation. The masses of bare states are defined as the *K*-matrix poles. The above-mentioned accumulation of widths of the primary states by one of the resonances due to mixing, was also observed in Ref. [14].

As the next step, the *K*-matrix analysis was extended to 1550 MeV [29], with the additional channels $\eta\eta$ and $\pi\pi\pi\pi$ included. The channel $\pi\pi\pi\pi$ is rather important for the correct description of spectra from 1300 to 1600 MeV, since $\sigma(\pi\pi \to \pi\pi\pi\pi)/\sigma(\pi\pi \to \pi\pi)$ is of the order of 0.5 at 1300 MeV and about 1.5 at 1500 MeV [31]. The use of the channels $\pi\pi$, $K\bar{K}$, and $\eta\eta$ provides an opportunity to perform the $q\bar{q}$ classification of bare 0^{++} states, f_0^{bare}, below 1600 MeV [29]. The point is that $q\bar{q}$-meson decays go to the new $q\bar{q}$ pair via the production of intermediate gluons. According to the rules of the $1/N$ expansion, the main contribution to the decay constant comes from planar diagrams. When an isoscalar $q\bar{q}$ meson disintegrates into two pseudoscalar mesons P_1P_2, namely,

$$\pi\pi\,, \quad K\bar{K}\,, \quad \eta\eta\,, \quad \eta\eta'\,, \quad \eta'\eta'\,, \tag{1.8}$$

the coupling constants can be determined, up to a common coefficient, by two factors. The first is the quark content of the $q\bar{q}$ meson:

$$q\bar{q} = n\bar{n}\cos\phi + s\bar{s}\sin\phi\,, \tag{1.9}$$

where $n\bar{n} = (u\bar{u} + d\bar{d})/\sqrt{2}$. The second is the parameter λ, which characterizes the relative probability of producing non-strange and strange quarks by gluons in soft processes:

$$u\bar{u} : d\bar{d} : s\bar{s} = 1 : 1 : \lambda\,. \tag{1.10}$$

Experimental data provide the following values for this parameter: $\lambda \simeq 0.5$ [32] in central hadron production in hadron–hadron high-energy collisions, $\lambda = 0.8 \pm 0.2$ [33] for the decays of tensor mesons and $\lambda = 0.6 \pm 0.1$ [34, 35] for the ratio of yields of η and η' mesons in the decays $J/\psi \to \gamma\eta/\gamma\eta'$.

The coupling constants for the decay $q\bar{q} \to P_1P_2$ into channels (1.8), which are defined by the leading planar diagrams in the $1/N$ expansion, may be presented as

$$g(q\bar{q} \to P_1P_2) = C_{P_1P_2}(\phi, \lambda) g^{\mathrm{L}}\,, \tag{1.11}$$

where $C_{P_1P_2}(\phi, \lambda)$ is a wholly calculable coefficient depending on the mixing angle ϕ and parameter λ; g^{L} is a common factor describing the unknown dynamics of the process. Therefore, experimental investigation of resonance decays into channels (1.8) allows us to reconstruct the quark content of the state (i.e. its mixing angle ϕ), thus making it possible to establish the meson systematics.

However, on the basis of the decay constant analysis, it is impossible to determine unambiguously whether we are dealing with a $q\bar{q}$ meson or with a glueball. The reason is that the glueball decay is a two-stage process, with the subsequent production of two $q\bar{q}$ pairs. After the production of the first $q\bar{q}$ pair, in the intermediate state a $q\bar{q}$ system exists with the following content:

$$n\bar{n}\cos\phi_{\mathrm{G}} + s\bar{s}\sin\phi_{\mathrm{G}}\,, \qquad \tan\phi_{\mathrm{G}} = \sqrt{\frac{\lambda}{2}}. \tag{1.12}$$

For $\lambda = 0.45–0.80$ the mixing angle is $\phi_{\mathrm{G}} = 25^\circ – 32^\circ$. At the second stage, the intermediate $q\bar{q}$ state (1.12) turns into the P_1P_2 mesons; this means that the relations between the glueball coupling constants are the same as for the decay of the $q\bar{q}$ meson with $\phi = \phi_{\mathrm{G}}$.

Analysis of the $\pi\pi$, $K\bar{K}$, and $\eta\eta$ spectra performed in Ref. [29] proved that in the region below 1600 MeV there are

four scalar–isoscalar states, and only one of them is an $s\bar{s}$-dominant state. Since each of the $^3P_0q\bar{q}$ multiplets contains two $I=0$ states, which refer to two flavor combinations, $n\bar{n}$ and $s\bar{s}$, then, as a result of the analysis of Ref. [29], the following dilemma becomes apparent:

(1) In the region 1000 – 1800 MeV there are three $^3P_0q\bar{q}$ nonets: the basic one, $1^3P_0q\bar{q}$, and two radial excitations, $2^3P_0q\bar{q}$ and $3^3P_0q\bar{q}$. In this case, there should exist two $s\bar{s}$-dominant scalar mesons in the region 1600 – 1800 MeV.

(2) At 1600 – 1800 MeV, there is only one $s\bar{s}$-dominant state. Then, one of the three mesons from the region 1200 – 1600 MeV is an extra one from the point of view of $q\bar{q}$ systematics, and it should be considered as a candidate for an exotic meson: the ratios of couplings to the channels (1.8) found in Ref. [29] provide the basis to consider it as the lightest scalar glueball.

Thus, after carrying out the analysis of Ref. [29], the immediate task was to extend the *K*-matrix analysis of the 00^{++} wave to the region 1600 – 1900 MeV. Such an extension suggested the inclusion of the $\eta\eta'$ channel into the fitting procedure; this has been done in Ref. [30], where the *K*-matrix analysis was performed in the mass region 500 – 1900 MeV, with the following five channels taken into consideration: $\pi\pi$, $K\bar{K}$, $\eta\eta$, $\pi\pi\pi\pi$, and $\eta\eta'$. It was shown that in the range 1600 – 1900 MeV there exists only one f_0 meson with a dominant $s\bar{s}$ component, hence the analysis [30] confirmed case (2). In this way, it was also shown that there are two variants for fixing the scalar glueball.

Solution I. Two bare states, $f_0^{\rm bare}(720\pm100)$ and $f_0^{\rm bare}(1260\pm30)$, are members of the multiplet $1^3P_0q\bar{q}$, and $f_0^{\rm bare}(720)$ is the $s\bar{s}$-rich state, with $\phi(720)=-69^\circ\pm12^\circ$. The bare states $f_0^{\rm bare}(1600\pm50)$ and $f_0^{\rm bare}(1810\pm30)$ are members of the $2^3P_0q\bar{q}$ nonet , and $f_0^{\rm bare}(1600)$ is dominantly $n\bar{n}$ state, with $\phi(1600)=-6^\circ\pm15^\circ$. The state $f_0^{\rm bare}(1235\pm50)$ is superfluous from the point of view of the $q\bar{q}$ classification; its coupling constants satisfy the ratios relevant to gluonium. Therefore, this state may be considered as a candidate for the lightest scalar glueball.

Solution II. The basic scalar nonet is the same as in Solution I. The members of the next nonet, $2^3P_0q\bar{q}$, are as follows: $f_0^{\rm bare}(1235\pm50)$ and $f_0^{\rm bare}(1810\pm30)$. Both these states contain a considerable admixture of the $s\bar{s}$ component: $\phi(1235)=42^\circ\pm10^\circ$ and $\phi(1810)=-53^\circ\pm10^\circ$. The state $f_0^{\rm bare}(1560\pm30)$ is an extra one from the point of view of $q\bar{q}$ systematics and it may be regarded as a good candidate for the lightest scalar glueball.

The existence of two variants corresponds to the impossibility of answering unambiguously, on the basis of the information on the decay channels (1.8), if we are dealing with a glueball or $q\bar{q}$ meson with a mixing angle $\phi=25^\circ-32^\circ$, as was stressed above.

Both *K*-matrix solutions, I and II, lead to practically identical positions of the amplitude poles in the complex mass plane. The amplitude has five poles:

Resonance:	Location of pole (MeV):
$f_0(980)$,	$1015\pm15-i(43\pm8)$,
$f_0(1300)$,	$1300\pm20-i(120\pm20)$,
$f_0(1500)$,	$1499\pm8-i(65\pm10)$,
$f_0(1750)$,	$1750\pm30-i(125\pm70)$,
$f_0(1530^{+90}_{-250})$,	$1530^{+90}_{-250}-i(560\pm140)$.

(1.13)

The broad resonance $f_0(1530^{+90}_{-250})$ is not a new object in meson physics: this is the one called $\epsilon(1300)$. A large width of $f_0(1530^{+90}_{-250})$ is due to the accumulation of widths of neighboring resonances.

A reliable and unambiguous identification of the scalar glueball must be based upon a complete reconstruction of the multiplets $1^3P_0q\bar{q}$ and $2^3P_0q\bar{q}$. Each of these nonets consists of two scalar–isoscalar states f_0, one isovector–scalar state a_0, and the scalar kaon K_0. As was stated above, it is reasonable to perform the nonet classification of highly-excited $q\bar{q}$ states in terms of bare states, which do not contain clouds of real mesons. The analysis [30] fixed four $f_0^{\rm bare}$ mesons, which are necessary for the construction of two nonets; the two lightest isotriplet resonances, $a_0(980)$ and $a_0(1450)$, are also known (see Ref. [9]). A full *K*-matrix analysis of the 10^{++} wave, [36], provided the following resonance masses:

$$a_0(980)\to(988\pm6)-i(46\pm10)\ \text{MeV},$$
$$a_0(1450)\to(1565\pm30)-i(146\pm20)\ \text{MeV}. \qquad (1.14)$$

It should be pointed out that in the Particle Data Group compilation [9] the mass of the second resonance is too low by about 100 MeV. Corresponding bare states are as follows:

$$a_0^{\rm bare}(964\pm16),\qquad a_0^{\rm bare}(1670\pm70). \qquad (1.15)$$

The identification of scalar resonances as members of the multiplets $1^3P_0q\bar{q}$ and $2^3P_0q\bar{q}$ always raised problems. Namely, according to Refs [9, 37], the masses of the two lightest kaons are $1429\pm4\pm5$ MeV and $1945\pm10\pm20$ MeV; these are noticeably higher than the average masses of other mesons which are candidates for the scalar-nonet members. This high position on the mass scale of the scalar kaon $K_0(1430)$ gave impetus to models where the basic $1^3P_0q\bar{q}$ multiplet was fixed in the region 1350 – 1500 MeV, and the resonances $f_0(980)$ and $a_0(980)$ were considered as exotic states — hadron molecules [38], multiquark bags [39], or minions [40, 41].

In Ref. [42] a *K*-matrix re-analysis of the S-wave $K\pi$ spectrum was carried out to determine the $K_0^{\rm bare}$. Another reason to re-analyse it was as follows. In Ref. [37] the $K\pi$ spectra were investigated in two separate mass regions, 820 – 1580 MeV and 1780 – 2180 MeV, but the mass region 1580 – 1780 MeV was not included into the analysis of the $K\pi$ amplitude. Our experience in fitting the 00^{++} wave [30] teaches us that separate consideration of different mass regions leads to the loss of certain information. In order to get a full picture, a simultaneous fit is needed; moreover, at 1580 – 1780 MeV there is a rapid change of the amplitude.

As follows from the *K*-matrix fit of the $IJ^P=\frac{1}{2}0^+$ wave [42], for a good description of the $K\pi$ spectrum in the region 800 – 2000 MeV at least two K_0 states are necessary. Correspondingly, the $\frac{1}{2}0^+$ amplitude of this minimal solution has poles near the physical region on the sheet II (under the $K\pi$ cut) and on the sheet III (under the $K\pi$ and $K\eta'$ cuts), at the following complex masses:

$$(1415\pm30)-i(165\pm25)\ \text{MeV},$$
$$(1820\pm40)-i(125\pm35)\ \text{MeV}. \qquad (1.16)$$

The $K\eta'$ threshold, being in the vicinity of the resonance (at 1458 MeV), strongly influences the $\frac{1}{2}0^+$ amplitude, so the lowest K_0 state has a second pole which is located above the $K\eta'$ cut, at $M=(1525\pm125)-i(420\pm80)$ MeV: the situa-

tion is analogous to that observed for the $f_0(980)$ meson, which also has a two-pole structure for the amplitude due to the $K\bar{K}$ threshold. The $K\eta$ channel weakly influences the $\frac{1}{2}0^+$ $K\pi$ amplitude: experimental data [37] prove it as well as the quark combinatorial rules.

The minimal solution contains two K_0^{bare} states:

$$K_0^{\text{bare}}(1200^{+60}_{-110}), \qquad K_0^{\text{bare}}(1820^{+40}_{-75}). \tag{1.17}$$

In this minimal solution, the lightest scalar bare kaon appears 200 MeV lower than the amplitude pole, and this latter circumstance makes it easier to build the basic scalar nonet, with masses in the range 900 – 1200 MeV.

It is worth noting that the $K\pi$ spectra also allow solutions with three poles, with much better χ^2; still, for these solutions the lightest kaon state, K_0^{bare}, does not leave the range 900 – 1200 MeV. In the tree-pole solution we have

$$K_0^{\text{bare}}(1090 \pm 40), \qquad K_0^{\text{bare}}(1375^{+125}_{-40}), \qquad K_0^{\text{bare}}(1950^{+70}_{-20}), \tag{1.18}$$

and the $K\pi$ amplitude has the poles:

$$\begin{aligned}
&\text{Sheet II} \;\; — \; M = 998 \pm 15 - i(80 \pm 15)\ \text{MeV};\\
&\text{Sheet II} \;\; — \; M = 1426 \pm 15 - i(182 \pm 15)\ \text{MeV};\\
&\text{Sheet III} \; — \; M = 1468 \pm 30 - i(309 \pm 15)\ \text{MeV};\\
&\text{Sheet III} \; — \; M = 1815 \pm 25 - i(130 \pm 25)\ \text{MeV}.
\end{aligned} \tag{1.19}$$

The state $K_0^{\text{bare}}(1375^{+125}_{-40})$, being near the $K\eta'$ threshold, results in doubling the amplitude poles around 1400 MeV. It should be underlined that masses of the lightest bare kaon states obtained by the two- and three-pole solutions coincide within the errors.

The K-matrix fit of the $\frac{1}{2}0^+$ $K\pi$ wave makes it possible to complete, in terms of bare states, the construction of the two lowest scalar nonets. In line with the result for the 00^{++} wave [30], where two solutions for an extra state (a candidate for the glueball) were found, there are two variants for the nonet classification of scalar mesons. The basic $1^3P_0q\bar{q}$ nonet is the same for both variants:

$$\begin{aligned}
&a_0^{\text{bare}}(960 \pm 30),\ f_0^{\text{bare}}(720 \pm 100),\\
&f_0^{\text{bare}}(1260^{+100}_{-30}),\ K_0^{\text{bare}}(1200^{+90}_{-150}).
\end{aligned} \tag{1.20}$$

It should be particularly stressed that the wave function $f_0^{\text{bare}}(720)$ in the flavor space is close to an octet one; indeed, $\phi(720) = -69^\circ \pm 12^\circ$, while $\phi_{\text{octet}} = -54.7^\circ$. Correspondingly, $f_0^{\text{bare}}(1260)$ is close to the flavor singlet. A similar situation is observed in the pseudoscalar sector where the flavor wave functions η and η' are close to octet and singlet ones. It is even more analogous, if one takes into consideration that the mass difference of isoscalar states in these sectors coincide with each other, and the scalar masses are not much larger than the corresponding masses of pseudoscalars, $m_s - m_{ps} \simeq (200 \pm 100)$ MeV. Such coincidences clearly point towards parity degeneration of the interaction forces in isoscalar channels.

Thus, one may conclude: the basic nonet of scalar mesons is uniquely fixed by the K-matrix fit of meson spectra. It is located rather low on the mass scale, in the range 750 – 1250 MeV. Here, at mass values below 1200 MeV, there is no room for exotic states.

The $2^3P_0q\bar{q}$ nonet contains the following states in Solution I:

$$\begin{aligned}
&a_0^{\text{bare}}(1640 \pm 40),\ f_0^{\text{bare}}(1600 \pm 50),\ f_0^{\text{bare}}(1810^{+30}_{-100}),\\
&K_0^{\text{bare}}(1375^{+125}_{-40}) \quad \text{or} \quad K_0^{\text{bare}}(1820^{+40}_{-60}).
\end{aligned} \tag{1.21}$$

An extra state with respect to the nonet classification is $f_0^{\text{bare}}(1235^{+150}_{-30})$.

In Solution II the $2^3P_0q\bar{q}$ nonet looks like

$$\begin{aligned}
&a_0^{\text{bare}}(1640 \pm 40),\ f_0^{\text{bare}}(1235^{+150}_{-30}),\ f_0^{\text{bare}}(1810^{+30}_{-100}),\\
&K_0^{\text{bare}}(1375^{+125}_{-40}) \quad \text{or} \quad K_0^{\text{bare}}(1820^{+40}_{-60}).
\end{aligned} \tag{1.22}$$

In this solution an extra state is $f_0^{\text{bare}}(1600 \pm 50)$; once again it should be stressed that the mass of this state appears just in the mass region where lattice calculations for the mass of the lightest scalar gluonium point; also the coupling constants for meson channels agree with the quark combinatorial ratios for the gluonium decay.

Immediately after performing the K-matrix analysis in the range up to 1900 MeV, the problem of presentation of the 00^{++} amplitude as a dispersion integral was raised. The dispersion N/D representation correctly restores the analytic properties of partial amplitude over the whole complex s-plane. In addition, and this is the principal point, within the dispersion representation it is possible to reconstruct the propagator matrix, thus evaluating the mixing of the $q\bar{q}$ states and the glueball, and then to restore correctly the gluonium mass. The dispersive N/D description of the wave 00^{++} was performed in Refs [6, 7]: in Ref. [6] the region 1200 – 1700 MeV, where three scalar–isoscalar states are located, was studied; then, in Ref. [7] the region under investigation was extended to 1900 MeV, with the fourth state, $f_0(1780)$, taken in consideration.

The results of the N/D representation of the 00^{++} wave allowed us to draw a picture of the mixing for the lowest scalar gluonium: it mixes with the two neighboring $q\bar{q}$ states — members of the multiplets 1^3P_0 and 2^3P_0, and the resonance, which is descendant of a pure glueball, accumulates large parts of the widths of the neighboring resonances, being transformed into the broad state $f_0\left(1530^{+90}_{-250}\right)$.

It should be emphasized that the state f_0^{bare}, which was found in the K-matrix fit, does not explicitly describe the gluodynamic glueball, for the state f_0^{bare} contains non-gluonic degrees of freedom related to real parts of the loop diagrams (imaginary parts are responsible for the decay process). The dispersion relation N/D method is able to restore the real and imaginary parts of the loop diagrams, thus providing a complete picture of the mixing, so it also restores the mass of gluonium. In Solution I it is equal to

$$m_{\text{gluonium}} = 1225\ \text{MeV} \tag{1.23}$$

and

$$m_{\text{gluonium}} = 1633\ \text{MeV} \tag{1.24}$$

in Solution II. The value (1.24) agree well with the mass values of the lightest scalar glueball obtained in lattice calculations.

It is rather striking that both solutions obtained in the dispersive technique provide practically the same structure for the 00^{++} wave and the quark – gluon content of physical

resonances: in both solutions the broad resonance, $f_0(1530^{+90}_{-250})$, is a descendant of the gluonium, keeping about 40 – 50% of its component, while the remnant part of the gluonium is shared between $f_0(1300)$ and $f_0(1500)$. From this point of view, the structure of resonances in the range 1300 – 1600 MeV is uniquely solved.

The formation of the broad state which is seen in the 00^{++} wave raises a question about the presence of such effects in other waves as well, for it is reasonable to believe that exotic mesons (glueballs and hybrids) with other quantum numbers can also afford a width accumulation. Because of that, the search for other exotic mesons must be inseparably linked with the study of broad resonances.

Another problem appears which is no less intriguing: the broad resonance, after having absorbed the widths of its neighboring resonances, plays the role of a locking state, since it prevents the decay of neighboring states with the same quantum numbers. This means that the broad resonance actually plays the role of a dynamic barrier for the nearby states. How does this dynamic barrier relate to the confinement barrier? — Only detailed investigations of broad resonances in other waves may answer this question.

2. *K* matrix and the dispersive *N*/*D* representation of the scattering amplitude

In this section a brief review is made of the technique used in the analysis of meson spectra. Namely, the analytic properties of the amplitude are discussed together with the connection of the dispersion N/D representation to the K-matrix approach. The role of short and large distances in the formation of meson spectra under investigation is also discussed, and in this connection the notion of a 'bare state' is introduced. The quark combinatorial relations between the coupling constants for the glueball decay to meson channels are considered in comparison with similar relations for $q\bar{q}$ states: these relations provide the basis for the nonet systematics of mesons.

2.1 Scattering amplitude, *T* matrix and *K* matrix

Using a simple example, let us get over the terminology and notations used for the analysis of meson spectra.

In terms of the wave function, which expresses the relative motion of two spinless particles, the scattering at large distances is described by incoming plane wave and outgoing spherical wave, $r^{-1}f(\theta)\exp(\mathrm{i}kr)$, with the coefficient related to the partial amplitudes as follows:

$$f(\theta)=\frac{1}{2\mathrm{i}k}\sum_{l=0}^{\infty}(2l+1)P_l(\cos\theta)\Big\{\exp\big[2\mathrm{i}\delta_l(k)\big]-1\Big\}. \quad (2.1)$$

This formula is written for one-channel scattering in the absence of absorbtion (k is the momentum of the relative motion, l is the angular momentum and θ is the scattering angle). The T-matrix element is determined by the scattering phase shift δ_l:

$$T_l=\frac{1}{2\mathrm{i}}\big[\exp(2\mathrm{i}\delta_l)-1\big]=\exp(\mathrm{i}\delta_l)\sin\delta_l. \quad (2.2)$$

For the investigation of analytic properties, it is suitable to use an amplitude with another normalization:

$$A_l=\frac{1}{2\mathrm{i}\rho(k)}\big[\exp(2\mathrm{i}\delta_l)-1\big], \quad (2.3)$$

where $\rho(k)$ is the invariant two-particle phase space factor:

$$\rho(k)=\int \mathrm{d}\Phi\,(P;k_1,k_2),$$

$$\mathrm{d}\Phi(P;k_1,k_2)=\frac{1}{2}\,\frac{\mathrm{d}^3k_1}{(2\pi)^3 2k_{10}}\,\frac{\mathrm{d}^3k_2}{(2\pi)^3 2k_{20}}(2\pi)^4\delta^{(4)}(P-k_1-k_2). \quad (2.4)$$

The invariant phase space factor is determined by three four-momenta: the total momentum of scattered particles, P, with $P^2=s$, and the momenta of particles 1 and 2, k_1 and k_2, respectively. For equal masses of particles 1 and 2, we get

$$\rho(k)=\frac{k}{8\pi\sqrt{s}}, \qquad k=\sqrt{\frac{s}{4}-m^2}. \quad (2.5)$$

The K-matrix representation of the amplitude A_l reads

$$A_l=\frac{K_l(k^2)}{1-\mathrm{i}\rho(k)K_l(k^2)}. \quad (2.6)$$

K_l is real in the physical region; the imaginary part of the amplitude is explicitly written in Eqn (2.6). In addition, K_l being a function of the invariant energy squared s, is analytic near the threshold singularity, $s=4m^2$; a singular term is singled out, it is explicitly given by the two-particle phase space factor ρ.

In the presence of absorbtion, the scattering is described by the absorbtion coefficient η_l inserted to the partial wave expansion (2.1):

$$\big[\exp(2\mathrm{i}\delta_l)-1\big]\to\big[\eta_l\exp(2\mathrm{i}\delta_l)-1\big]. \quad (2.7)$$

Here $0\leqslant\eta_l\leqslant 1$; the case $\eta_l=0$ corresponds to full absorbtion.

It is suitable to display the energy-dependent amplitude T_l on the Argand diagram, which is an appropriate instrument for searching resonances. The T-matrix element at fixed k (or s) corresponds to a point on the plane $(\mathrm{Re}\,T_l,\mathrm{Im}\,T_l)$. As a function of k, it draws a trajectory on the circle with a radius of $1/2$ and center at the point $(0,\mathrm{i}/2)$. In the inelasticity case, the trajectory T_l enters the internal part of the circle.

The K-matrix representation of the amplitude with an absorbtion requires fixing the inelastic channels. Consider the inelasticity occurring due to another two-particle channel; we denote these channels by the indices 1 and 2. Then the elastic scattering amplitude $1+1'\to 1+1'$ (denoted as A_{11}; the index of the partial wave l is omitted) can be represented in the form of Eqn (2.6):

$$A_{11}=\frac{K(k^2)}{1-\mathrm{i}\rho_1K(k^2)}. \quad (2.8)$$

However, the block $K(k^2)$ has an imaginary part above the threshold of the second channel:

$$K(k^2)=K_{11}+\mathrm{i}\,\frac{K_{12}\,\rho_2K_{21}}{1-\mathrm{i}\rho_2K_{22}}. \quad (2.9)$$

Here ρ_2 is phase space factor of the second channel $2+2'$, and the matrix elements K_{11}, $K_{12}=K_{21}$ and K_{22} are real functions of k^2 in the physical region. The threshold singularities of channels 1 and 2, which are located at $s=(m_1+m_1')^2$ (threshold of channel 1) and at $s=(m_2+m_2')^2$

(threshold of channel 2), are explicitly written in Eqns (2.8) and (2.9) — they are present in the phase space factors ρ_1 and ρ_2, respectively. The function $K(k^2)$ is real below the threshold of the second channel, $(m_1+m_1')^2 < s < (m_2+m_2')^2$, because in this region $\rho_2 = \mathrm{i}|\rho_2|$.

2.2 Dispersion relation N/D method and the K-matrix representation

The dispersion relation N/D method [43] correctly reproduces the analytic properties of the amplitude on the whole s-plane. Following Refs [44, 45], we present here the elements of this method which are used in the analysis of meson spectra.

The partial amplitude $A(s)$ (as before, the index l is omitted for brevity) is written in the form of the ratio

$$A(s) = \frac{N(s)}{D(s)}\,, \tag{2.10}$$

$N(s)$ is a function of the complex variable s. It has only left-hand side singularities of the amplitude, which are related to the interaction forces, i.e. to the diagrams with meson exchanges in the crossing channels (Fig. 1). These singularities are located on the left of the threshold singularities, at $s = (m_1+m_1')^2 - m^2_{\mathrm{crossing}}$.

The D-function contains only right-hand side singularities, which result from the rescattering of particles in the s-channel. Figure 1 shows the corresponding rescattering processes.

First, we consider the one-channel case, with equal particle masses $m_1 = m_1'$. In this case the D-function assumes the following form:

$$D(s) = 1 - B(s)\,, \qquad B(s) = \int_{4m^2}^{\infty} \frac{\mathrm{d}s'}{\pi}\,\frac{N(s')\rho(s')}{s'-s-\mathrm{i}0}\,. \tag{2.11}$$

Here the index 1 is omitted: $m_1 \to m$, $\rho_1 \to \rho$. The form of Eqn (2.11) suggests that $D(s) \to 1$ at $s \to \infty$ [more generally, $D(s) \to$ const at $s \to \infty$, since this case can be reduced to Eqn (2.11) by the re-definition of $N(s)$]. Moreover, in Eqn (2.11) it is also suggested that the D-function does not contain the Castillejo–Dalitz–Dyson poles (a detailed description of the N/D method may be found in Refs [43, 44]).

Representation of the N-function in the form of a sum of separable vertex functions [44] is likely to be a reasonable ansatz: this technique is successfully applied to the description of the nucleon–nucleon scattering amplitude [45]; in addition, the technique is elaborated for the presentation of the t-channel exchange diagrams as a sum of separable vertex functions [46]. For the simplest case, which is discussed below, $N(s) = g^2(s)$. Then

$$A(s) = \frac{g^2(s)}{1-B(s)}\,, \qquad B(s) = \int_{4m^2}^{\infty} \frac{\mathrm{d}s'}{\pi}\,\frac{g(s')\rho(s')g(s')}{s'-s-\mathrm{i}0}\,. \tag{2.12}$$

Expanding Eqn (2.12) in a series with respect to $B(s)$, we represent the amplitude $A(s)$ as a sum of the diagrams shown in Figs 2a–2c, etc.; $B(s)$ in Eqn (2.12) is a loop diagram. At $s > 4m^2$, the loop diagram is a complex quantity:

$$\mathrm{Im}\,B(s) = g^2(s)\rho(s)\,, \qquad \mathrm{Re}\,B(s) = P\int_{4m^2}^{\infty} \frac{\mathrm{d}(s')}{\pi}\,\frac{g^2(s')\rho(s')}{s'-s}\,. \tag{2.13}$$

The amplitude (2.12) stands for the case when the partial wave amplitude does not contain input particles: the bound states, if any, are formed by particle interaction taken in the N-function. The inclusion of input particles into the amplitude corresponds to the assumption of $D(s)$ increasing as $s \to \infty$. The linearly growing $D(s)$ can be written in the form

$$D(s) = m_0^2 - s - B(s)\,, \qquad B(s) = \int_{4m^2}^{\infty} \frac{\mathrm{d}(s')}{\pi}\,\frac{g^2(s')\rho(s')}{s'-s-\mathrm{i}0}\,. \tag{2.14}$$

The amplitude

$$A(s) = \frac{g^2(s)}{m_0^2 - s - B(s)} \tag{2.15}$$

is an infinite set of diagrams shown in Figs 2d–2f, etc.; $B(s)$ stands for the loop diagram and $(m_0^2-s)^{-1}$ is the propagator of the input particle.

The K-matrix representation of the $A(s)$ amplitude is related to the explicit separation of the imaginary part of the loop diagram:

$$A(s) = \frac{g^2(s)}{m_0^2 - s - \mathrm{Re}\,B(s) - \mathrm{i}\rho(s)g^2(s)} = \frac{K(s)}{1-\mathrm{i}\rho(s)K(s)}\,,$$
$$K(s) = \frac{g^2(s)}{m_0^2 - s - \mathrm{Re}\,B(s)}\,. \tag{2.16}$$

In the two-particle loop diagram, the function $\mathrm{Re}\,B(s)$ is analytical at the point $s = 4m^2$. This means that poles are the only singularities of $K(s)$ in the physical region. However, in the left half-plane s, $K(s)$ has singularities related to the t-channel exchanges.

The poles of the amplitude $A(s)$, which are determined by the condition

$$m_0^2 - s - B(s) = 0\,, \tag{2.17}$$

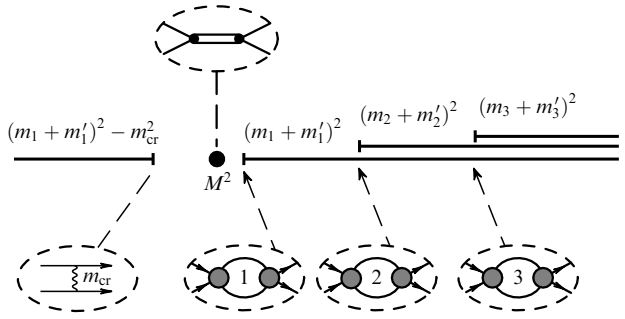

Figure 1. Complex s-plane and positions of singularities of the partial amplitude: the right-hand singularities at $s \geqslant (m_1+m_1')^2$ are due to elastic and inelastic rescatterings, the left-hand ones are due to the interaction forces, that is, particle exchanges in the crossing channels.

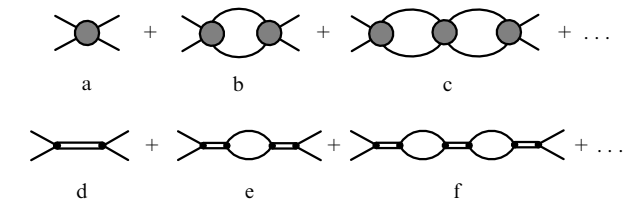

Figure 2. Diagrams representing s-channel scattering.

are related to particles with quantum numbers of the partial wave under consideration. If the pole is above the threshold, at $s = 4m^2$, we are dealing with the resonance; this very case is studied further. Let the equality (2.17) be satisfied at the point

$$s = M^2 \equiv \mu^2 - i\Gamma\mu\,. \tag{2.18}$$

Expanding the real part of the denominator (2.15) in a series near $s = \mu^2$, one has

$$m_0^2 - s - \operatorname{Re} B(s) \simeq \bigl[1 + \operatorname{Re} B'(\mu^2)\bigr](\mu^2 - s) - ig^2(s)\rho(s)\,. \tag{2.19}$$

The standard Breit – Wigner approximation comes when $\operatorname{Im} B(s)$ is fixed at the point $s = \mu^2$. If the pole is located not far from the threshold singularity $s = 4m^2$, it is necessary to keep the s-dependence in the phase space factor, and we use the modified Breit – Wigner formula:

$$A(s) = \frac{\gamma}{\mu^2 - s - i\gamma\rho(s)}\,, \qquad \gamma = \frac{g^2(\mu^2)}{1 + \operatorname{Re} B'(\mu^2)}\,. \tag{2.20}$$

A similar resonance approximation may be also carried out for the K-matrix amplitude representation, that corresponds to the expansion for $K(s)$ given by Eqn (2.16) near the point $s = \mu^2$:

$$K(s) = \frac{g^2(K)}{\mu^2 - s} + f. \tag{2.21}$$

Here

$$g^2(K) = \frac{g^2(\mu^2)}{1 + \operatorname{Re} B'(\mu^2)}\,,$$
$$f = \frac{g^2(\mu^2)}{2\bigl[1 + \operatorname{Re} B'(\mu^2)\bigr]} - \frac{2g(\mu^2)g'(\mu^2)}{1 + \operatorname{Re} B'(\mu^2)}\,. \tag{2.22}$$

2.3 Multichannel scattering

The resonance amplitude (2.15) can be easily generalized for the case of n channels. The corresponding transition amplitude $b \to a$ is

$$A_{ab}(s) = \frac{g_a(s)g_b(s)}{m_0^2 - s - B(s)}\,, \qquad B(s) = \sum_{c=1}^{n} B_{cc}(s)\,, \tag{2.23}$$

where B_{cc} is defined by the standard expression [see Eqn (2.14)] with the properly chosen phase space factor, vertex function and integration region:

$$g^2(s')\rho(s') \to g_c^2(s')\rho_c(s')\,, \qquad 4m^2 \to 4m_c^2\,. \tag{2.24}$$

The transition amplitudes A_{ab} form a matrix $\hat{A}$. The amplitude written in the K-matrix representation reads:

$$\hat{A} = \hat{K}\,\frac{I}{I - i\hat{\rho}\hat{K}}\,, \tag{2.25}$$

where $\hat{K}$ is the $n \times n$ matrix, $K_{ab}(s) = K_{ba}(s)$, I is the unit $n \times n$ matrix, $I = \operatorname{diag}(1, 1, \ldots, 1)$, and $\hat{\rho}$ is the diagonal matrix of phase space factors:

$$\hat{\rho} = \operatorname{diag}\bigl(\rho_1(s), \rho_2(s), \ldots, \rho_n(s)\bigr)\,. \tag{2.26}$$

The K-matrix elements are

$$K_{ab}(s) = \frac{g_a(s)g_b(s)}{m_0^2 - s - \operatorname{Re} B(s)}\,. \tag{2.27}$$

In the vicinity of the resonance, the K-matrix elements may be expanded in a series: in this case we have a representation of the K-matrix elements similar to that of Eqn (2.21).

2.4 $q\bar{q}$ mesons: the problem of small and large distances

The $q\bar{q}$ classification of meson states in the vicinity of 1000 – 2000 MeV faces the problem of quark – hadron duality as well as a tightly related problem of separating large- and small-distance interactions contributing to the formation of meson spectra.

Let us discuss these problems using the language of the standard quark model. In this model the $q\bar{q}$ levels are determined by the potential which increases infinitely with r, $V(r) \propto \alpha r$ (Fig. 3a). An infinitely rising potential creates an infinite set of $q\bar{q}$ levels. However, it is obvious that the standard quark model is a simplified picture, since only the lowest $q\bar{q}$ levels are stable with respect to hadron decays. The heavier states decay by hadron channels: an excited $(q\bar{q})_a$ state produces a new $q\bar{q}$ pair, then the $(q\bar{q})_a + (q\bar{q})$ quarks recombine into mesons, which leave the confinement trap with the formation of a continuous meson spectrum. This structure is conventionally shown in Fig. 3b, where the interaction related to the confinement is shown as a certain potential barrier, namely, the interaction at $r < R_{\text{confinement}}$ creates the discrete levels of $q\bar{q}$ spectra, while the transitions into the region $r > R_{\text{confinement}}$ give rise to the continuous meson spectrum. This very meson spectrum is observed in the experiment. This problem of reconstruction of the $q\bar{q}$ levels created at $r < R_{\text{confinement}}$ is directly related to the determination of the effect of the meson decay spectra on the level shift: the classification of $q\bar{q}$ levels requires the elimination of the decay products of real mesons.

The K-matrix representation of the amplitude resolves the problem of excluding the components of real mesons; formally, it corresponds to the limit $\rho_a \to 0$ in Eqn (2.25). If only leading pole singularities are taken into account, the transition amplitude $b \to a$ assumes the form

$$A_{ab}^{\text{bare}}(s) = K_{ab}(s) = \frac{g_a(K)g_b(K)}{\mu^2 - s} + f_{ab}\,. \tag{2.28}$$

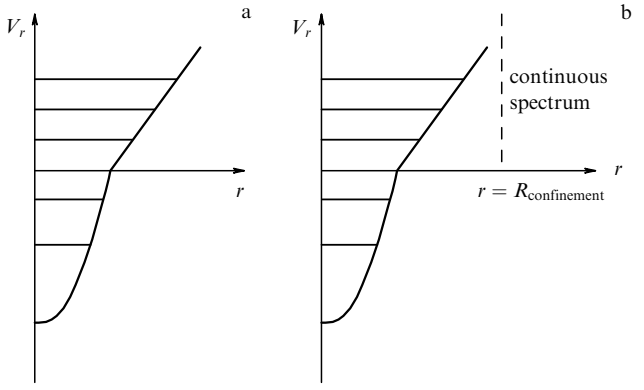

Figure 3. (a) The standard quark model potential with stable $q\bar{q}$ levels. (b) The potential with unstable highly excited levels, corresponding to the realistic situation for $q\bar{q}$ states.

Thus, the K-matrix pole corresponds to the state with the removed cloud of real mesons. For this reason, we call the corresponding states 'bare mesons' [29, 30]. However, one should distinguish between this notation and that of 'bare particles' of field theory, where a cloud includes virtual mass-off-shell particles as well.

In the case when the $q\bar{q}$ spectrum contains several states with the same quantum numbers, the amplitude $A_{ab}^{\text{bare}}(s)$ is determined by the sum of the corresponding poles:

$$A_{ab}^{\text{bare}}(s) = \sum_{\alpha} \frac{g_a^{(\alpha)}(K) g_b^{(\alpha)}(K)}{\mu_\alpha^2 - s} + f_{ab} \,. \tag{2.29}$$

Representation of the amplitude responsible for the interaction at $r < R_{\text{confinement}}$ in the form of a series of poles is not new: it was widely used in dual models for leading contributions in the $1/N_c$ expansion. From the point of view of these models, the s-independent term f_{ab} is the total contribution of poles which are distant from the region under consideration.

Coupling constants of the bare state, $g_a^{(\alpha)}(K)$, are a source of information on the quark – gluon content of this state.

2.5 Coupling constants of the gluonium and $q\bar{q}$ states to meson channels: the rules of the $1/N$ expansion and quark combinatorial relations

The quark – gluon content of states related to the K-matrix poles (bare states) is revealed in the relations between couplings of these poles to meson channels, $g_a^{(\alpha)}$.

First, let us evaluate these coupling constants using the rules of $1/N$ expansion; this evaluation will be done both for the transitions *glueball → two mesons* and for the transitions $q\bar{q}$ *state → two mesons*. For this purpose, we consider the gluon loop diagram which corresponds to the two-gluon self-energy part: *glueball → two gluons → glueball* (Fig. 4a). This loop diagram is of the order of unity, provided the glueball is a two-gluon composite particle: $B(G \to gg \to G) \sim g_{G\to gg}^2 N_c^2 \sim 1$, where $g_{G\to gg}$ is the coupling constant of a glueball to two gluons. Therefore,

$$g_{G\to gg} \sim \frac{1}{N_c} \,. \tag{2.30}$$

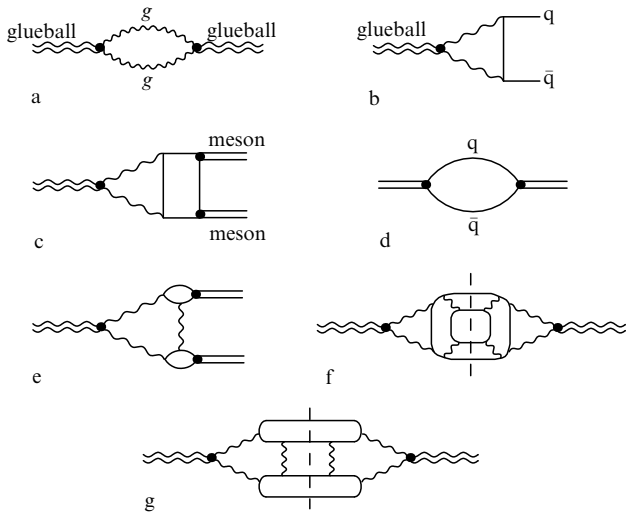

Figure 4. Diagrams for a glueball decay into two mesons.

The coupling constant for the transition $g_{G\to q\bar{q}}$ is determined by the diagrams of Fig. 4b. A similar evaluation gives:

$$g_{G\to q\bar{q}} \sim g_{G\to gg}\, g_{QCD}^2 N_c \sim \frac{1}{N_c} \,. \tag{2.31}$$

Here g_{QCD} is the quark – gluon coupling constant, which is of the order of $1/\sqrt{N_c}$ [8]. The coupling constant for the transition *glueball → two mesons* in the leading $1/N_c$ terms is governed by the diagrams of Fig. 4c:

$$g_{G\to mm}^{L} \sim g_{G\to q\bar{q}}\, g_{m\to q\bar{q}}^2 N_c \sim \frac{1}{N_c} \,. \tag{2.32}$$

Here the approximate equality $g_{m\to q\bar{q}} \sim 1/\sqrt{N_c}$ is used which follows from the fact that the loop diagram of the meson propagator (see Fig. 4d) is of the order of unity: $B(m \to q\bar{q} \to m) \sim g_{m\to q\bar{q}}^2 N_c \sim 1$. A diagram of Fig. 4e-type governs the coupling constants for the transition *glueball → two mesons* in the next-to-leading terms of the $1/N_c$ expansion:

$$g_{G\to mm}^{NL} \sim g_{G\to gg}\, g_{QCD}^4 g_{m\to q\bar{q}}^2 N_c^2 \sim \frac{1}{N_c^2} \,. \tag{2.33}$$

As was mentioned above, the glueball can decay into channels (1.8). In this way, the production of light quarks by gluons occurs with a violation of the flavor blindness, $u\bar{u} : d\bar{d} : s\bar{s} = 1 : 1 : \lambda$. Within such an assumption, the coupling constants for the transition *glueball → two pseudoscalar mesons* can be calculated using quark combinatorial rules. These rules were successfully applied to the calculation of yields of secondary particles in the hadron – hadron high energy collisions [47] and to the decay $J/\psi \to$ hadrons [48]. The calculation of coupling constants for the decays *glueball → mesons* has been carried out in Refs [20, 34, 49].

The glueball decay constants to channels (1.8) are given in Table 1 for the leading, $g_{G\to mm}^{L}$, and next-to-leading, $g_{G\to mm}^{NL}$, terms of the $1/N$ expansion. The unknown dynamics of the

Table 1. Coupling constants for a glueball decaying into two pseudoscalar mesons, in the leading and next-to-leading terms of the $1/N$ expansion. Θ is the mixing angle for $\eta - \eta'$ mesons: $\eta = n\bar{n}\cos\Theta - s\bar{s}\sin\Theta$ and $\eta' = n\bar{n}\sin\Theta + s\bar{s}\cos\Theta$.

Channel	Coupling constants in the leading term of the $1/N$ expansion	Coupling constants in the next-to-leading term of the $1/N$ expansion	Identity factor
$\pi^0\pi^0$	G_L	0	$\frac{1}{2}$
$\pi^+\pi^-$	G_L	0	1
K^+K^-	$\sqrt{\lambda}\, G_L$	0	1
K^0K^0	$\sqrt{\lambda}\, G_L$	0	1
$\eta\eta$	$G_L(\cos^2\Theta + \lambda\sin^2\Theta)$	$2G_{NL}\left(\cos\Theta - \sqrt{\frac{\lambda}{2}}\sin\Theta\right)^2$	$\frac{1}{2}$
$\eta\eta'$	$G_L(1-\lambda)\sin\Theta\cos\Theta$	$2G_{NL}\left(\cos\Theta - \sqrt{\frac{\lambda}{2}}\sin\Theta\right) \times \left(\sin\Theta + \sqrt{\frac{\lambda}{2}}\cos\Theta\right)$	1
$\eta'\eta'$	$G_L(\sin^2\Theta + \lambda\cos^2\Theta)$	$2G_{NL}\left(\sin\Theta + \sqrt{\frac{\lambda}{2}}\cos\Theta\right)^2$	$\frac{1}{2}$

decay is hidden in the parameters $G_{\rm L}$ and $G_{\rm NL}$. The decay constant to the channel n is a sum of both contributions:

$$g^{\rm L}_{{\rm G}\to{\rm mm}}(n)+g^{\rm NL}_{{\rm G}\to{\rm mm}}(n)\,. \tag{2.34}$$

The second term is suppressed, as compared to the first one, by a factor of $N_{\rm c}$; experience in the calculation of quark diagrams teaches us that this suppression is of the order of $1/10$.

The sum of coupling constants squared satisfies the sum rules:

$$\sum_n\left[g^{\rm L}_{{\rm G}\to{\rm mm}}(n)\right]^2 I(n)=\frac{1}{2}\,G^2_{\rm L}(2+\lambda)^2\,,$$

$$\sum_n\left[g^{\rm NL}_{{\rm G}\to{\rm mm}}(n)\right]^2 I(n)=\frac{1}{2}\,G^2_{\rm NL}(2+\lambda)^2\,, \tag{2.35}$$

where $I(n)$ is an identity factor for the particles produced (see Table 1). These sum rules follow from the quark – hadron duality: the sum of squared coupling constants over the whole set of flavor states is equivalent to the sum of cut diagrams with the quark loops (diagrams of the type of Fig. 4f for the leading and of the type of Fig. 4g for next-to-leading terms). Each quark loop contains the factor $(2+\lambda)$ related to the summation over light flavors [see Eqn (1.10)].

Quark combinatorial rules may be applied to the calculation of couplings of $(q\bar q)_a$ mesons to pseudoscalar channels (1.8). There exist two types of transitions $(q\bar q)_a$ *state* $\to$ *two mesons*: they are shown in Fig. 5. The type of process represented by the diagram of Fig. 5a is leading according to the rules of $1/N$ expansion; its coupling constant is of the order of

$$g^{\rm L}_{{\rm m}(a)\to{\rm mm}}\sim g^3_{{\rm m}\to{\rm q\bar q}}N_{\rm c}\sim\frac{1}{\sqrt{N_{\rm c}}}\,. \tag{2.36}$$

The decay constant for the process of Fig. 5b is of the order of

$$g^{\rm NL}_{{\rm m}(a)\to{\rm mm}}\sim g^3_{{\rm m}\to{\rm q\bar q}}N^2_{\rm c}g^4_{{\rm m}\to{\rm q\bar q}}\sim\frac{1}{N_{\rm c}\sqrt{N_{\rm c}}}\,. \tag{2.37}$$

The coupling constants for the decays $(q\bar q)_a\to\pi\pi$, $K\bar K$, $\eta\eta$, $\eta\eta'$, and $\eta'\eta'$ are shown in Table 2 both for the leading and next-to-leading orders; $g^{\rm L}$ and $g^{\rm NL}$ are the parameters, in which the unknown dynamics of the soft decay is hidden. Concerning the glueball decay, the coupling constant for the $(q\bar q)_a$-meson decay to the channel n is the sum of two terms:

$$g^{\rm L}_{{\rm m}(a)\to{\rm mm}}(n)+g^{\rm NL}_{{\rm m}(a)\to{\rm mm}}(n)\,. \tag{2.38}$$

These two terms in Eqn (2.38) define the decay constant of the $(q\bar q)_a$ meson in the general case: different variants of fixing the ratios of coupling constants correspond to different choices of the ratio $g^{\rm L}$ to $g^{\rm NL}$. Examples of different fixations of $g^{\rm L}/g^{\rm NL}$ may be found in Refs [40, 49].

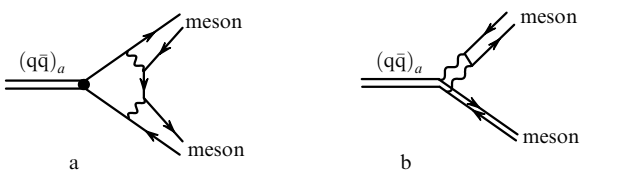

Figure 5. Diagrams for the decay of the $(q\bar q)_a$ state into two mesons.

Table 2. Coupling constants for a $q\bar q$ meson decaying into two pseudoscalar mesons in the leading and next-to-leading terms of the $1/N$ expansion. ϕ is the mixing angle for $n\bar n$ and $s\bar s$ states [see Eqn (1.9)].

Channel	Coupling constants in the leading term of the $1/N$ expansion	Coupling constants in the next-to-leading term of the $1/N$ expansion
$\pi^0\pi^0$	$g^{\rm L}\cos\dfrac{\phi}{\sqrt2}$	0
$\pi^+\pi^-$	$g^{\rm L}\cos\dfrac{\phi}{\sqrt2}$	0
K^+K^-	$\dfrac{g^{\rm L}(\sqrt2\sin\phi+\sqrt\lambda\cos\phi)}{\sqrt8}$	0
K^0K^0	$\dfrac{g^{\rm L}(\sqrt2\sin\phi+\sqrt\lambda\cos\phi)}{\sqrt8}$	0
$\eta\eta$	$g^{\rm L}\left(\cos^2\Theta\cos\dfrac{\phi}{\sqrt2}+\sqrt\lambda\sin\phi\sin^2\Theta\right)$	$\sqrt2\,g^{\rm NL}\left(\cos\Theta-\sqrt{\dfrac{\lambda}{2}}\sin\Theta\right)\times(\cos\phi\cos\Theta-\sin\phi\sin\Theta)$
$\eta\eta'$	$g^{\rm L}\sin\Theta\cos\Theta\left(\cos\dfrac{\Phi}{\sqrt2}-\sqrt\lambda\sin\phi\right)$	$\sqrt{\dfrac12}\,g^{\rm NL}\left[\left(\cos\Theta-\sqrt{\dfrac{\lambda}{2}}\sin\Theta\right)\times(\cos\phi\sin\Theta+\sin\phi\cos\Theta)+\left(\sin\Theta+\sqrt{\dfrac{\lambda}{2}}\cos\Theta\right)\times(\cos\phi\sin\Theta-\sin\phi\cos\Theta)\right]$
$\eta'\eta'$	$g^{\rm L}\left(\sin^2\Theta\cos\dfrac{\phi}{\sqrt2}+\sqrt\lambda\sin\Phi\cos^2\Theta\right)$	$\sqrt2\,g^{\rm NL}\left(\sin\Theta+\sqrt{\dfrac{\lambda}{2}}\cos\Theta\right)\times(\cos\phi\cos\Theta+\sin\phi\sin\Theta)$

Let us stress once again that the coupling constant ratios for the $(q\bar q)_a$ states (see Table 2) become identical to those of the glueball, when $\phi=\arctan\sqrt{\lambda/2}$: this is valid for leading and next-to-leading contributions. Therefore, on the basis of a study of couplings to the hadron decay channels only, it is impossible to distinguish between a glueball and an $I=0$ $(q\bar q)_a$ meson with the mixing angle $\phi\approx30^\circ$.

3. *K*-matrix analysis of meson spectra and the nonet classification of $q\bar q$ states

In this section the results obtained in Refs [30, 36, 42] for the waves 00^{++}, 10^{++}, 02^{++}, 12^{++}, and $\frac12 0^+$ are presented. On the basis of this analysis, the nonet classification of $q\bar q$ states is established.

3.1 *K*-matrix fit of 00^{++} wave: the spectra $\pi\pi$, $K\bar K$, $\eta\eta$, and $\eta\eta'$

To describe the spectra, in Ref. [30] the standard K-matrix representation of the 00^{++} amplitude (2.25) was used, where K_{ab} is a 5×5 matrix $(a,b=1,2,\ldots,5)$, with the following notations for channels: $1=\pi\pi$, $2=K\bar K$, $3=\eta\eta$, $4=\eta\eta'$, $5=(\pi\pi\pi\pi+$ *other multi-meson states*).

The matrix elements K_{ab} are parametrized in a form similar to Eqn (2.28):

$$K_{ab}=\left(\sum_\alpha\frac{g^{(\alpha)}_a g^{(\alpha)}_b}{M^2_\alpha-s}+f_{ab}\,\frac{1\ {\rm GeV}^2+s_0}{s+s_0}\right), \tag{3.1}$$

with the restriction $s_0\geqslant1\ {\rm GeV}^2$.

The following formulae provide the description of the spectra $\pi\pi$, $\eta\eta$ and $\eta\eta'$, obtained by GAMS group for the reactions with a t-channel pion exchange:

$$A_{\pi N\to Nb} = g(\bar\psi_N\gamma_5\psi_N)F(t)D(t)K_{1a}(t)(1-i\hat\rho\hat K)^{-1}_{ab}\,, \quad (3.2)$$

$$K_{1a}(t) = \left(\Sigma_\alpha \frac{g_1^{(\alpha)}(t)g_a^{(\alpha)}}{M_\alpha^2 - s} + f_{1a}(t)\,\frac{1\ \mathrm{GeV}^2 + s_0}{s+s_0}\right). \quad (3.3)$$

Here $D(t)$ is the pion propagator, $F_N(t)$ is the nucleon formfactor related to the vertex πNN, and $g_1^{(\alpha)}(t)$ and $f_{1a}(t)$ are the formfactors of the pion block.

The part of the amplitude for the reaction $p\bar p$ (*at rest*) $\to \pi^0\pi^0\pi^0$, $\pi^0\eta\eta$, which describes the formation of two mesons in the 00^{++} state, is written as follows:

$$A_{p\bar p\to \mathrm{mesons}} = A_1(s_{23}) + A_2(s_{13}) + A_3(s_{12})\,. \quad (3.4)$$

The amplitude $A_k(s_{ij})$ corresponds to the process with the 'last interaction' of particles ij, while the particle k remains a spectator.

The amplitude $A_1(s_{23})$ for the spectra $\pi\pi$ and $\eta\eta$ has the following form ($b = \pi\pi$, $\eta\eta$):

$$A_1(s_{23}) = K_{p\bar p\pi,a}(s_{23})(1-i\rho K)^{-1}_{ab}\,,$$

$$K_{p\bar p\pi,a}(s_{ij}) = \left(\sum_\alpha \frac{\Lambda_{p\bar p\pi}^{(\alpha)}\, g_a^{(\alpha)}}{M_\alpha^2 - s_{ij}} + \phi_{p\bar p\pi,a}\,\frac{1\ \mathrm{GeV}^2 + s_0}{s_{ij}+s_0}\right). \quad (3.5)$$

In the reaction $p\bar p$ (*at rest*) $\to \pi^0\pi^0\pi^0$, the amplitude is symmetric with respect to permutation of pion indices, i.e. $A_1(s_{ij}) = A_2(s_{ij}) = A_3(s_{ij})$. The $\pi^0\pi^0$ interaction in the reaction $p\bar p$ (*at rest*) $\to \pi^0\pi^0\eta$ is determined as follows (below $b = \pi\pi$):

$$A_1(s_{23}) = K_{p\bar p\eta,a}(s_{23})(1-i\rho K)^{-1}_{ab}\,,$$

$$K_{p\bar p\eta,a}(s_{ij}) = \left(\sum_\alpha \frac{\Lambda_{p\bar p\eta}^{(\alpha)}\, g_a^{(\alpha)}}{M_\alpha^2 - s_{ij}} + \phi_{p\bar p\eta,a}\,\frac{1\ \mathrm{GeV}^2 + s_0}{s_{ij}+s_0}\right). \quad (3.6)$$

The parameters $\Lambda^\alpha_{p\bar p\pi}$, $\phi_{p\bar p\pi}$, $\Lambda_{p\bar p\eta}$, and $\phi_{p\bar p\eta}$ can be complex magnitudes with different phases, that follows from the three-particle interaction; a more detailed discussion of the amplitude $p\bar p \to$ *three mesons* is given in Ref. [50].

3.2 Results of the *K*-matrix fit for the 00^{++} wave in the region below 1900 MeV

A simultaneous K-matrix fit of the 00^{++} spectra in the mass region 550–1900 MeV performed in Ref. [30] pointed to the existence of five bare states, f_0^{bare}. Only two of them, $f_0^{bare}(720)$ and $f_0^{bare}(1810)$, contain a large $s\bar s$ component. This means that only two $^3P_0q\bar q$ nonets can be built in the mass region below 1900 MeV.

The following requirements provide the basis for the nonet classification of bare states:

(1) nonet partners are orthogonal in flavor space, i.e. they must have mixing angle differences [see Eqn (1.9)] equal to 90°: $\phi_1 - \phi_2 = 90°$ (for this value the corridor $90° \pm 5°$ is allowed);

(2) the coupling constants g^L and g^{NL} (see Table 2) are approximately equal for the nonet partners: $g_1^L \simeq g_2^L$ and $g_1^{NL} \simeq g_2^{NL}$.

The standard quark model requires the equality of coupling constants. However, the s-dependent vertex functions and loop diagrams violate this equality because of the presence of mass differences of nonet partners. Moreover, the K-matrix coupling constants have an additional s-dependent factor $\left[1 + B'(s)\right]^{-1}$ [see Eqn (2.22)]. This factor strongly affects the region of small masses (the region of basic 1^3P_0 nonet), where the thresholds and left-hand singularities of partial amplitude play a more important role.

Fitting to experimental data (1.4)–(1.7) resulted in two solutions, I and II. First, let us sum up the results for Solution I.

Type of state:	Flavour wave function:
$f_0^{bare}(720) \to 1^3P_0q\bar q$	$0.40n\bar n - 0.92s\bar s$
$f_0^{bare}(1260) \to 1^3P_0q\bar q$	$0.92n\bar n + 0.40s\bar s$
$f_0^{bare}(1600) \to 2^3P_0q\bar q$	$0.995n\bar n - 0.10s\bar s$
$f_0^{bare}(1810) \to 2^3P_0q\bar q$	$0.10n\bar n + 0.995s\bar s$
$f_0^{bare}(1235) \to$ glueball $\to$	$0.91n\bar n + 0.42s\bar s$.

(3.7)

In Eqn (3.7) the 'flavor wave function' is introduced for the glueball. It describes the flavor content of the intermediate state for the glueball decay, see Fig. 4c.

Now let us summarize the results for Solution II.

Type of state:	Flavour wave function:
$f_0^{bare}(720) \to 1^3P_0q\bar q$	$0.40n\bar n - 0.92s\bar s$
$f_0^{bare}(1260) \to 1^3P_0q\bar q$	$0.92n\bar n + 0.40s\bar s$
$f_0^{bare}(1235) \to 2^3P_0q\bar q$	$0.74n\bar n + 0.67s\bar s$
$f_0^{bare}(1810) \to 2^3P_0q\bar q$	$0.67n\bar n - 0.74s\bar s$
$f_0^{bare}(1600) \to$ glueball $\to$	$0.91n\bar n + 0.42s\bar s$.

(3.8)

The quality of the data description by Solutions I and II can be seen in Figs 6 to 9 (dashed and solid curves, respectively).

3.3 The resonances: are they bumps or dips in the spectra?

For decades the search for meson resonances meant the search for bumps in the particle spectra. Only recently the understanding came that it is not always so, and the resonance $f_0(980)$ provides us with an example. In the peripheral $\pi\pi$ spectra it reveals itself as a dip, and a number of papers were devoted to this phenomenon (see, for example, Refs [9, 51]). The study of the 00^{++} wave proved that meson resonances in the region 1000–1600 MeV appear not only as bumps or dips, but also shoulders in the spectra. The fundamental characteristic of a resonance is not to be a bump or a dip in the spectrum, but to provide a circle on the Argand diagram.

Figures 10 and 11 demonstrate the Argand diagrams relevant to the fits of spectra under discussion. In Fig. 10 one can see the 00^{++} amplitudes $A_{\pi\pi\to\pi\pi}$, $A_{\pi\pi\to K\bar K}$, $A_{\pi\pi\to\eta\eta}$, and $A_{\pi\pi\to\eta\eta'}$ as functions of the energy. Indeed, rather distinct circles were obtained for the resonances $f_0(980)$, $f_0(1300)$, $f_0(1500)$, and $f_0(1780)$. The manifestation of the resonances $f_0(980)$ and $f_0(1300)$ in the form of circles is rather clear for the amplitudes $A_{\pi(t)\pi\to\pi\pi}$ at large $|t|$ (see Fig. 11).

3.4 Resonance $f_0(980)$: is it the $K\bar K$ molecule or the descendant of the lightest scalar $q\bar q$ states?

This is a principal problem for the $q\bar q$ systematics, which was first investigated in Ref. [14] using a K-matrix analysis for the

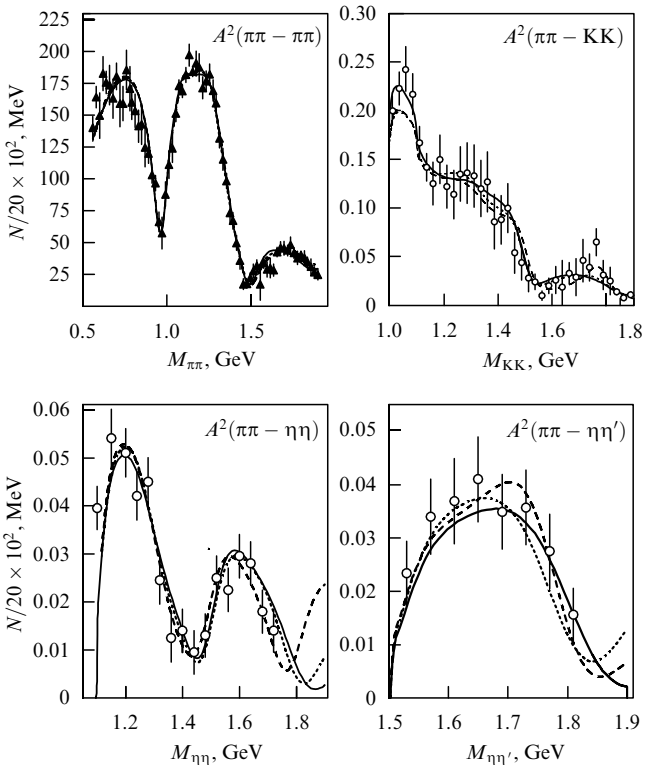

Figure 6. S-wave amplitudes squared and their description in Ref. [30]. The solid curve stands for Solution II.

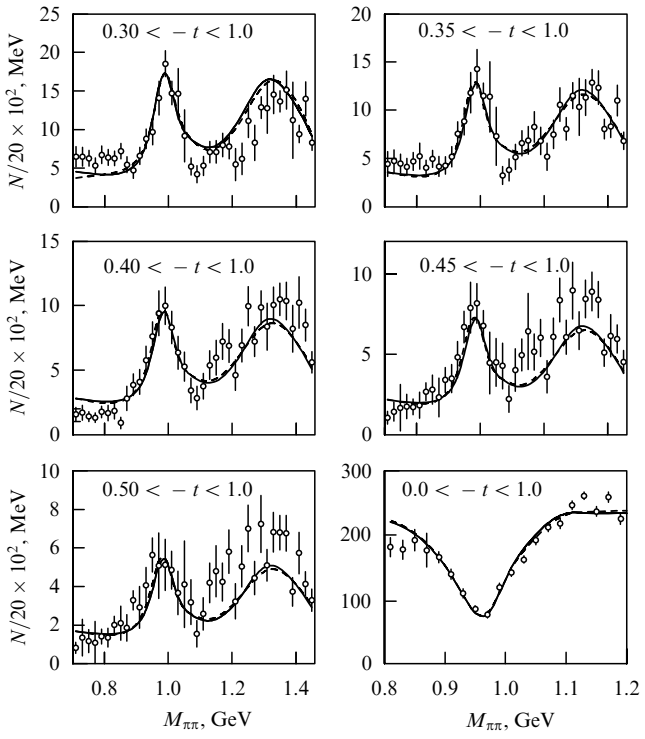

Figure 7. Event numbers for the reaction $\pi^- p \to \pi^0\pi^0 n$ versus the invariant mass of the $\pi\pi$ system selected at various intervals of the momentum transfer squared t. The solid curve stands for Solution II, the dashed one for Solution I.

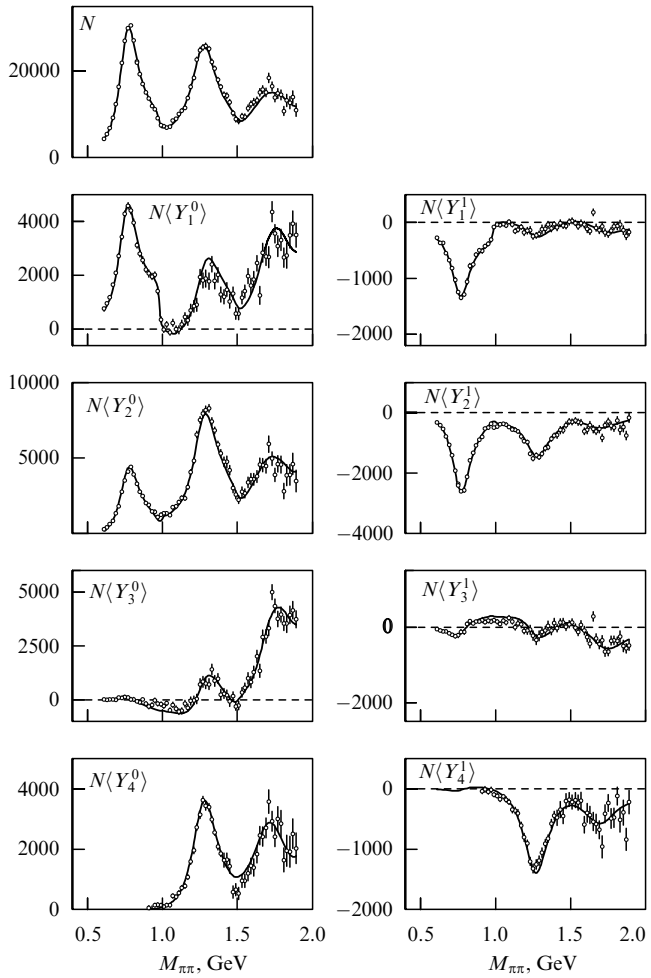

Figure 8. Description of the angle moments for the $\pi\pi$ distributions measured in the reaction $\pi^- p \to n\pi^-\pi^+$ [27]; the curve stands for Solution II [30].

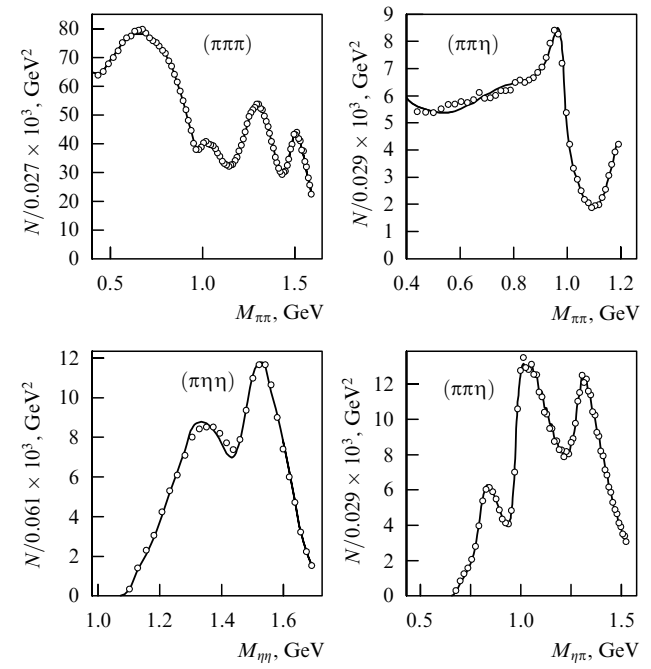

Figure 9. $\pi^0\pi^0$ spectra in the reactions $p\bar{p} \to \pi^0\pi^0\pi^0$, $p\bar{p} \to \eta\pi^0\pi^0$; the $\eta\eta$ spectrum in the reaction $p\bar{p} \to \pi^0\eta\eta$ and the $\eta\pi^0$ spectrum in the reaction $p\bar{p} \to \pi^0\pi^0\eta$. The curves correspond to Solution II [30].

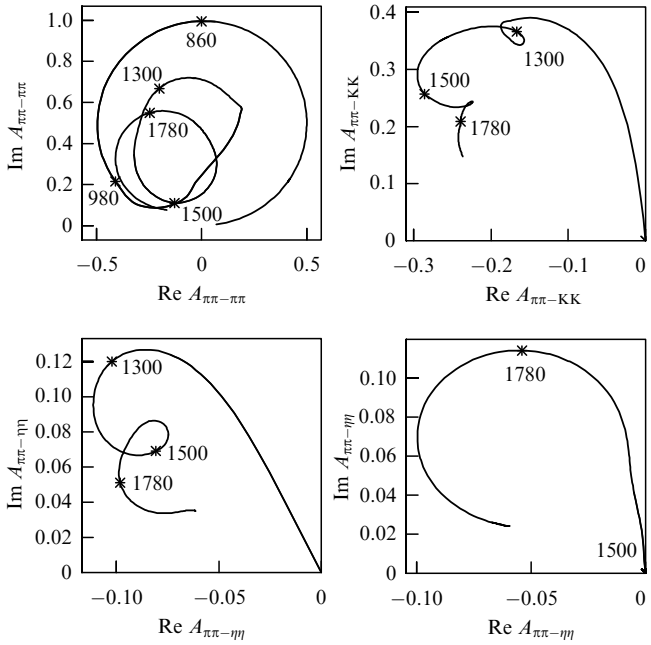

Figure 10. Argand diagram for the unitary S-wave amplitudes in the reactions $\pi\pi \to \pi\pi$, $\pi\pi \to K\bar{K}$, $\pi\pi \to \eta\eta$, and $\pi\pi \to \eta\eta'$ [30].

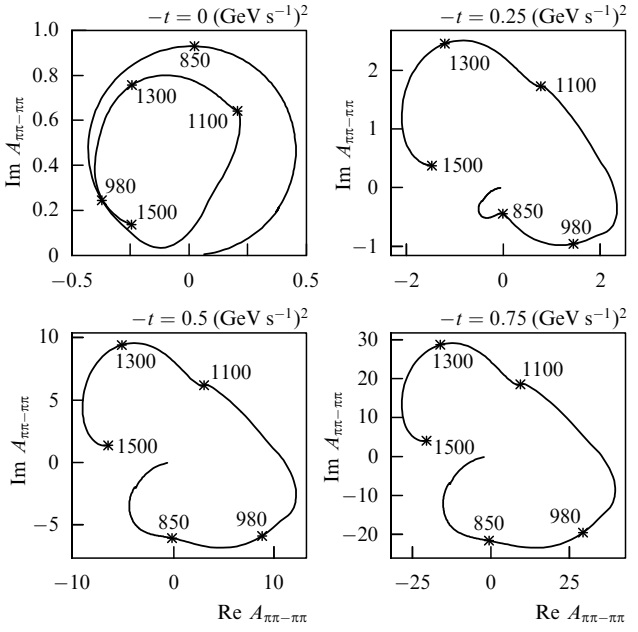

Figure 11. Argand diagram for the isoscalar S-wave $\pi\pi(t) \to \pi\pi$ scattering amplitude [30] at different momentum transfers squared t.

low-energy part of the 00^{++} wave. Following this paper, we provide arguments that $f_0(980)$ is the descendant of the lightest $q\bar{q}$ states.

The two poles correspond to the resonance $f_0(980)$, with the following complex masses: $M = 1015 - i46$ MeV on the second sheet (under the $\pi\pi$ cut) and $M = 936 - i238$ MeV on the third sheet (under the $\pi\pi$ and $K\bar{K}$ cuts). The second pole, at $936 - i238$ MeV, appears because of a well-known doubling of poles affected by the proximity of the $K\bar{K}$ threshold (see, for example, Refs [51, 52]). The first pole at $1015 - i46$ MeV dominates in the $\pi\pi$ spectrum, providing a sharp dip in the $\pi\pi \to \pi\pi$ spectrum or a bump in the spectrum $\pi\pi(t) \to \pi\pi$ at large $|t|$ [24]. Let us study the dynamics of this pole, when the decays into the channels $1 = \pi\pi$ and $2 = K\bar{K}$ are subsequently switched on and off. To this end, let us substitute the following into the K-matrix amplitude:

$$g_1(720) \to \xi_1 g_1(720)\,, \qquad g_2(720) \to \xi_2 g_2(720)\,, \tag{3.9}$$

with ξ_a varying over the interval $0 \leqslant \xi_a \leqslant 1$. At $\xi_1 \to 0$ and $\xi_2 \to 0$ the decay channels for the lightest 00^{++} state are switched off, and we are dealing with the 'bare' state, in terms of Refs [29, 30]. At $\xi_1 = \xi_2 = 1$ the real case is restored. At $\xi_1 \simeq \xi_2 \simeq 0$ the mass of the bare state is in the vicinity of 720 MeV, while, with the increase of ξ_a, the lightest scalar state acquires the components of real mesons, $\pi\pi$ and $K\bar{K}$, and, due to transitions to these states, it mixes with the other scalar ones. As a result, the mass of the lightest scalar state increases approaching the region around 1000 MeV. At $\xi_1 = \xi_2 = 1$, the pole of the amplitude is at

$$M(\textit{real case}) = 1015 - i46 \text{ MeV}\,, \tag{3.10}$$

i.e. near the $K\bar{K}$ threshold. Therefore, the $K\bar{K}$ component is of the quasi-molecular type: the relative momentum of K mesons is small, hence the mean distance between the K mesons is comparatively large. However, one can see that the $K\bar{K}$ component weakly affects the formation of the final state. Indeed, let us switch off the $K\bar{K}$ state, i.e. let us put in the amplitude $\xi_1 = 1$ and $\xi_2 = 0$. Then, the pole appears at the point

$$M(\textit{without } K\bar{K}) = 979 - i53 \text{ MeV}\,. \tag{3.11}$$

Actually the mass shift

$$M(\textit{real case}) - M(\textit{without } K\bar{K}) = 36 + i7 \text{ MeV} \tag{3.12}$$

is comparatively small, thus making the role of the $K\bar{K}$ component in the formation of the real $f_0(980)$ state insignificant.

Therefore, the K-matrix analysis of 00^{++} wave restores the following picture of the formation of $f_0(980)$. Before mixing, there existed the lightest scalar–isoscalar $q\bar{q}$ state $f_0^{\text{bare}}(720 \pm 100)$, with the flavor wave function close to the octet one:

$$\psi_{\text{flavor}}(720) = \cos\theta_S\,\psi_8 - \sin\theta_S\,\psi_1\,, \qquad \theta_S = 14^\circ \pm 12^\circ\,, \tag{3.13}$$

$$\psi_1 = \frac{1}{\sqrt{3}}(u\bar{u} + d\bar{d} + s\bar{s})\,, \qquad \psi_8 = \frac{1}{\sqrt{6}}(u\bar{u} + d\bar{d}) - \sqrt{\frac{2}{3}}\,s\bar{s}\,. \tag{3.14}$$

The mixing with other states, which goes through the transition $f_0^{\text{bare}}(720) \to \pi\pi$, leads to the formation of a resonance with characteristics which are almost the same as observed in the experiment [see Eqn (3.11)]. The onset of the $K\bar{K}$ component, $f_0^{\text{bare}}(720) \to K\bar{K}$, effects a relatively small shift of mass and width [see Eqn (3.12)].

It should be noted that direct measurements also point out that $f_0(980)$ has considerable short distance components: the production of $f_0(980)$ is not suppressed in the reaction $\pi^- p \to f_0(980)p$ at large momentum transfers [24, 53] as well as in radiative J/ψ decay [54].

One should pay attention to the fact that the lightest pseudoscalar–isoscalar state, that is, the η meson, also has flavor wave function close to the octet one: $\eta = \cos\theta_{\rm P}\,\psi_8 - \sin\theta_{\rm P}\,\psi_1$ with $\theta_{\rm P} = -16.7^\circ \pm 2.8^\circ$ [12].

3.5 The wave $IJ^{\rm PC} = 10^{++}$

Two isovector–scalar resonances are clearly seen in reactions (1.4) [18, 19]. The lightest of them is the well-known $a_0(980)$, while the next resonance is the recently discovered $a_0(1450)$ (according to Ref. [9], its mass is 1450 ± 40 MeV and the width $\Gamma = 270 \pm 40$ MeV). Note that fitting to the latest high statistics data [30, 36, 56] provided us with a greater mass value: 1520 ± 40 MeV.

For a description of the scalar–isoscalar amplitude, in Ref. [36] the two-pole 4×4 K matrix was used, with the channel notations: $1 = \pi\eta$ $2 = K\bar{K}$, $3 = \pi\eta'$, $4 = \textit{multi-meson states}$. The couplings to the two-meson channels are defined by the quark combinatorial relations (see Table 3). We recall that the constants $g^{\rm L}$ are the same for all multiplet members. At the first stage of the fit, the coupling constants of the lightest resonance a_0 were varied over the interval limited by the constants $g^{\rm L}[f_0^{\rm bare}(720)]$ and $g^{\rm L}[f_0^{\rm bare}(1260)]$. In all variants of the fit the coupling constant $g^{\rm L}[a_0^{\rm bare}(\textit{lightest state})]$ was found to be rather close to $g^{\rm L}[f_0^{\rm bare}(1260)]$; so in the final variant of the fit these coupling constants were taken as equal to each other. The coupling constants of the next isovector–scalar resonance to two mesons were also fixed to be equal to each other for all 2^3P_0-multiplet members.

The fit allowed us to find two solutions for the wave 10^{++}, which practically coincide for the resonance sector and differ for background terms. The positions of the amplitude poles and relevant bare states are shown in Eqns (1.14) and (1.15).

In Ref. [41], a hypothesis was discussed that the resonances $a_0(980)$ and $f_0(980)$ belong to a special class of states (minions), which are loosely bound to hadron channels: the small widths of $a_0(980)$ and $f_0(980)$ were considered as arguments in favor of this particular nature. The characteristics of resonance $a_0(980)$ provide a good opportunity to check this hypothesis: actually the components of real mesons yielded by the decays of $a_0(980)$ into $\pi\eta$ and $K\bar{K}$ weakly affect this state [see Eqns (1.14) and (1.15)]. The K-matrix fit of the data [36] proved that $g^{\rm L}[f_0^{\rm bare}(964)]$ is not small, being of the order of a standard hadronic value, and the small width of $a_0(980)$ is related not to the small probability of the decay, as could follow from the minion nature of $a_0(980)$, but to the threshold effect. It should be emphasized that this result is also seen in the T-matrix analysis of the data [19, 56].

Table 3. Coupling constants for the transitions $K_0^0 \to \textit{two mesons}$ and $a^- \to \textit{two mesons}$ in the leading and next-to-leading terms of the $1/N$ expansion.

Channel	Coupling constants in the leading terms	Coupling constants in the next-to-leading terms
$K^+\pi^-$	$\dfrac{g^{\rm L}}{2}$	0
$K^0\pi^0$	$-\dfrac{g^{\rm L}}{\sqrt{8}}$	0
$K^0\eta$	$\left(\cos\dfrac{\Theta}{\sqrt{2}} - \sqrt{\lambda}\sin\Theta\right)\dfrac{g^{\rm L}}{2}$	$\left(\sqrt{2}\cos\Theta - \sqrt{\lambda}\sin\Theta\right)\dfrac{g^{\rm NL}}{2}$
$K^0\eta'$	$\left(\sin\dfrac{\Theta}{\sqrt{2}} + \sqrt{\lambda}\cos\Theta\right)\dfrac{g^{\rm L}}{2}$	$\left(\sqrt{2}\cos\Theta - \sqrt{\lambda}\sin\Theta\right)\dfrac{g^{\rm NL}}{2}$
K^-K^0	$\dfrac{g^{\rm L}\sqrt{\lambda}}{2}$	0
$\pi^-\eta$	$\dfrac{g^{\rm L}\cos\Theta}{\sqrt{2}}$	$\left(\sqrt{2}\cos\Theta - \sqrt{\lambda}\sin\Theta\right)\dfrac{g^{\rm NL}}{2}$
$\pi^-\eta'$	$\dfrac{g^{\rm L}\sin\Theta}{\sqrt{2}}$	$\left(\sqrt{2}\sin\Theta - \sqrt{\lambda}\cos\Theta\right)\dfrac{g^{\rm NL}}{2}$

3.6 *K*-matrix analysis of the Kπ S-wave

A partial-wave analysis of the $K^-\pi^+$ system for the reaction $K^-p \to K^-\pi^+n$ at 11 GeV s^{-1} has been carried out in Ref. [37], where two alternative solutions (A and B), which differ only in the region above 1800 MeV, were found for the S-wave. In paper [37] the T-matrix fit for the Kπ S-wave was performed as well, though independently for the regions 850 – 1600 MeV and 1800 – 2100 MeV. In the first region, the resonance $K_0^*(1430)$ was found:

$$M_{\rm R} = 1429 \pm 9\ \text{MeV}\,, \qquad \Gamma = 287 \pm 31\ \text{MeV}\,. \tag{3.15}$$

In the second mass region, Solutions A and B provided the following parameters for the description of the resonance $K_0^*(1950)$:

$$\begin{aligned} &\text{Solution A:} \quad M_{\rm R} = 1934 \pm 28\ \text{MeV}\,, \quad \Gamma = 174 \pm 98\ \text{MeV}\,,\\ &\text{Solution B:} \quad M_{\rm R} = 1955 \pm 18\ \text{MeV}\,, \quad \Gamma = 228 \pm 56\ \text{MeV}\,. \end{aligned} \tag{3.16}$$

The necessity of improving this analysis is obvious. Firstly, the mass region 1600 – 1800 MeV, where the amplitude varies quickly, must be included into the consideration. As was stressed above, it is well-known that, due to the strong interference, a resonance may reveal itself not only as a bump in the spectrum but also as a dip or a shoulder: likewise, resonances appear in the 00^{++} wave. Secondly, the interference effects are also the source of ambiguities. It is worth noting that the ambiguities in the 00^{++} wave were successfully removed in Refs [30, 36], that was due only to a simultaneous fit of different meson spectra. For the wave $\frac{1}{2}0^+$, the data available are not copious, therefore one may suspect that the solution found in Ref. [37] is not unique.

The K-matrix re-analysis of the Kπ S-wave has been carried out in Ref. [42], with the purpose of:

(i) restoring masses and coupling constants of the bare states for the wave $\frac{1}{2}0^+$, in order to establish the $q\bar{q}$ classification;

(ii) finding out all possible K-matrix solutions for the Kπ S-wave in the mass region up to 2000 MeV.

The S-wave Kπ scattering amplitude extracted from the reaction $K^-p \to K^-\pi^+n$ for small momentum transfers is a sum of two components with isotopic spins 1/2 and 3/2:

$$A_{\rm S} = A_{\rm S}^{1/2} + \frac{1}{2}\,A_{\rm S}^{3/2} = |A_{\rm S}|\exp(i\phi_{\rm S})\,, \tag{3.17}$$

where $|A_{\rm S}|$ and $\phi_{\rm S}$ are measurable quantities entering the S-wave amplitude [37]. The S-wave part of the amplitude with isotopic spin $I = 3/2$ has a non-resonance-type behavior at the energies under consideration, so it may be parametrized as follows:

$$A_{\rm S}^{3/2}(s) = \frac{\rho_{K\pi}(s)a_{3/2}(s)}{1 - i\rho_{K\pi}(s)a_{3/2}(s)}\,, \tag{3.18}$$

where $a_{3/2}(s)$ is a smooth function and $\rho_{K\pi}(s)$ is the Kπ phase space factor.

For the description of the $A_{\rm S}^{1/2}$ amplitude, the 3×3 K matrix was used in Ref. [42], with the following channel

notations: $1 = K\pi, 2 = K\eta', 3 = K\pi\pi\pi$ + *multi-meson states*. Accounting for the $K\eta$-channel does not affect the description of the data, for the transition $K\pi \to K\eta$ is suppressed [37], that also agrees with quark combinatorial results (see Table 3). In Ref. [42] the fit of the wave $\frac{1}{2}0^+$ was performed with the parametrization of K_{ab} given in Eqn (3.1). For the reaction $K^-p \to K^-\pi^+n$ the data analysed with small momentum transfers ($|t| < 0.2$ GeV^2) were singled out , and at the first stage the data were fitted to the unitary amplitude (3.1). At the next stage, the t-dependence of the K-matrix amplitude was taken into consideration. The amplitude $K\pi(t) \to K\pi$ [$\pi(t)$ labels virtual pion] is equal to $A_S^{1/2} = K_{1a}(t)\,(I - i\rho K)^{-1}_{a1}$: the parametrization of the matrix $K_{1a}(t)$ is given in Eqn (3.3).

The coupling constants are determined from the quark combinatorial rules, they are presented in Table 3. In Ref. [42] only the leading terms in the $1/N$ expansion were taken into consideration: in this case coupling constants are fixed by the fit of the 00^{++} and 10^{++} waves, because g^L is a common parameter for all the nonet members.

The description of the $\frac{1}{2}0^+$ wave was performed under two assumptions, namely, with the two- and three-pole structure of the wave in the mass region below 2000 MeV.

In Ref. [37], two solutions, A and B, were found for the wave $\frac{1}{2}0^+$; they differ at $M_{\pi K} > 1800$ MeV only. Correspondingly, in Ref. [42] the two two-pole K-matrix solutions, (A-1) and (B-1), were obtained. The positions of the amplitude poles are practically the same for both solutions; they are given by Eqn (1.16). The description of data is shown in Fig. 12. The mass of the first resonance in Eqn (1.16) does not strongly differ from that of Ref. [37] [see Eqn (3.15)], but the width for the resonance found in the K-matrix solution is half that. This follows from the correct accounting for the $K\eta'$ threshold in the K-matrix solution and relevant doubling of poles. The mass of the second resonance in the K-matrix solution decreased, as compared to the value of Ref. [37], by more than 100 MeV.

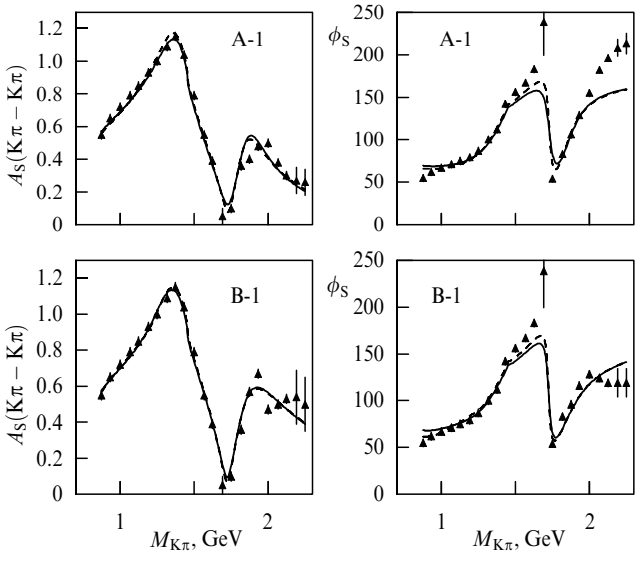

Figure 12. Description of data in Ref. [37] in the two-pole K-matrix fit: Solutions (A-1) and (B-1). The solid curves correspond to the solution found for unitary amplitude; the dashed lines stand for the fit with the t-dependent K matrix; ϕ_S is in degrees.

The masses of bare kaon states related to the two-pole solution are given in Eqn (1.17). The mass of the lightest state is 1200^{+60}_{-110} MeV, i.e. this scalar kaon is located in the same mass region as the other scalars — candidates for the basic 1^3P_0-nonet members.

The description of data in the three-pole K-matrix fit is shown in Fig. 13. The high mass range, $M_{K\pi} > 1700$ MeV, is described in Solutions (A-2) and (B-2) by the two poles. However, the two-pole structure of the amplitude did not change the characteristics of the two first resonances — they are identical to Solutions (A-2) and (B-2). In Solution (B-3) the region $M_{K\pi} < 1600$ MeV is described by two poles. The positions of bare states in Solution (B-3) are given in Eqn (1.18) and the corresponding positions of poles in Eqn (1.19).

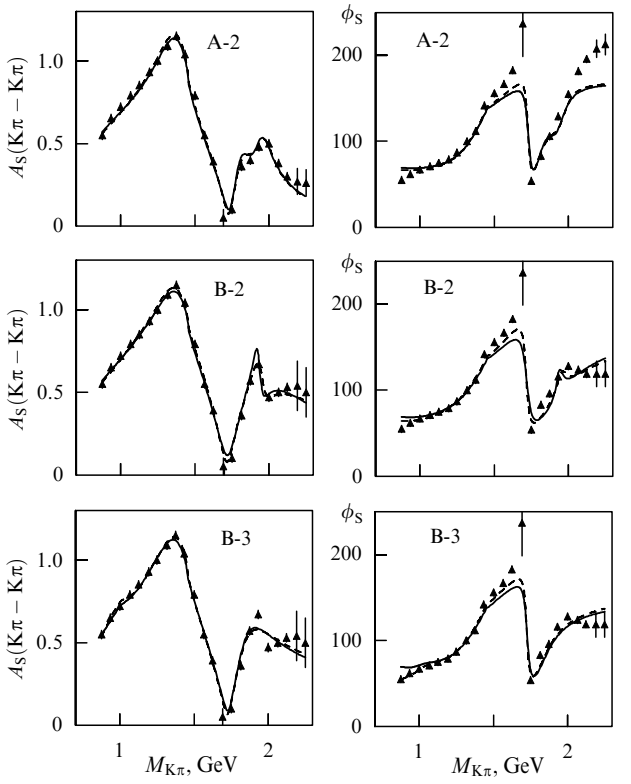

Figure 13. Description of data in Ref. [37] in the three-pole K-matrix fit: Solutions (A-2), (B-2) and (B-3); ϕ_S is in degrees.

The solid curves in Figs 12 and 13 represent the description of the $K\pi$ wave by the unitary amplitude, and the dashed lines correspond to the fits performed with the t-dependent $K\pi$ amplitude. It is seen that the t-dependence allows us to get a better description of the phase shifts around 1700 MeV. It should be noted that in this region, as well as in the mass region above 2000 MeV for Solution A, the data under consideration violate the unitary limit. It is hardly possible that the rather strong violation of unitarity is a consequence of the amplitude t-dependence; more likely it is related to the underestimation of systematic errors in the partial-wave analysis of Ref. [37] in those regions. The t-dependence included in the fitting procedure does not strongly affect the masses of the bare states and the positions of the amplitude poles. As a rule, the masses of bare states found in the t-dependent fit are 20–30 MeV less than the masses obtained in the t-independent fits.

4. Propagator matrix: the analysis of the $IJ^{PC} = 00^{++}$ wave

Here we are summing the results of the analysis of the 00^{++} wave performed in Refs [6, 7], in terms of the propagator matrix (D matrix). The D-matrix technique is based on the dispersion relation N/D method, allowing us to reconstruct the amplitude, which is analytical over the whole complex s-plane. We discuss the effects which are due to resonance overlapping and mixing; namely, the mass shifts and accumulation of widths by one of the neighboring resonances. An expansion of the physically observed states in a series with respect to initial (non-mixed) states is performed.

The investigation is made using the 00^{++} wave, but the method can be easily generalized for the other waves by using the technique developed in Refs [44, 45].

4.1 The mixing of two unstable states

In the case of two resonances, the propagator of state 1 is determined by the diagrams of Fig. 14a. Having all these processes accounted for, the propagator of state 1 is

$$D_{11}(s) = \left(m_1^2 - s - B_{11}(s) - \frac{B_{12}(s)B_{21}(s)}{m_2^2 - s - B_{22}(s)} \right)^{-1} . \quad (4.1)$$

Here m_1 and m_2 are the masses of the input states 1 and 2, and the loop diagrams $B_{ij}(s)$ are defined by Eqn (2.21), with the substitution $g^2(s) \to g_i(s)g_j(s)$. It will be helpful to introduce the propagator matrix D_{ij}, where the nondiagonal elements $D_{12} = D_{21}$ correspond to the transitions $1 \to 2$ and $2 \to 1$ (see Fig. 14b). The matrix reads:

$$\hat{D} = \begin{vmatrix} D_{11} & D_{12} \\ D_{21} & D_{22} \end{vmatrix} = \frac{1}{(M_1^2 - s)(M_2^2 - s) - B_{12}B_{21}} \begin{vmatrix} M_2^2 - s & B_{12} \\ B_{21} & M_1^2 - s \end{vmatrix} . \quad (4.2)$$

Here the following notation is used:

$$M_i^2 = m_i^2 - B_{ii}(s) , \qquad i = 1, 2 . \quad (4.3)$$

The zeros of the denominator of the propagator matrix (4.2) define the complex resonance masses after the mixing:

$$\Pi(s) = (M_1^2 - s)(M_2^2 - s) - B_{12}B_{21} = 0 . \quad (4.4)$$

We denote the complex masses of mixed states by M_A and M_B.

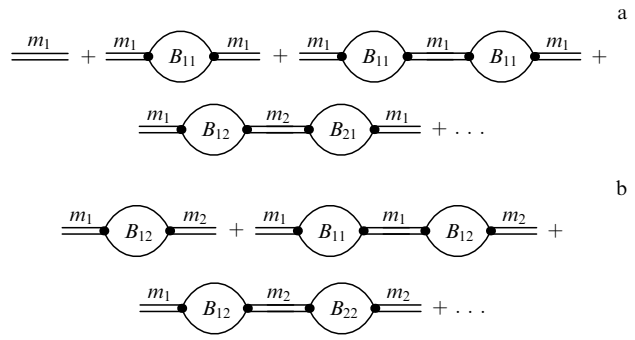

Figure 14. Diagrams describing the propagation functions D_{11} (a) and D_{12} (b) for the interaction of two bare states.

Let us consider a simple model, where the s-dependence of the function $B_{ij}(s)$ near the points $s \sim M_A^2$ and $s \sim M_B^2$ is assumed to be negligible. M_i^2 and B_{12} being constants, we have:

$$M_{A,B}^2 = \frac{1}{2}(M_1^2 + M_2^2) \pm \sqrt{\frac{1}{4}(M_1^2 - M_2^2)^2 + B_{12}B_{21}} . \quad (4.5)$$

In the case when the widths of the initial resonances 1 and 2 are small (hence the imaginary part of the transition diagram B_{12} is also small), Eqn (4.5) turns into the standard formula of quantum mechanics for the split of mixing levels, which become repulsive as a result of mixing. Then

$$\hat{D} = \begin{vmatrix} \dfrac{\cos^2\theta}{M_A^2 - s} + \dfrac{\sin^2\theta}{M_B^2 - s} & \dfrac{-\cos\theta\sin\theta}{M_A^2 - s} + \dfrac{\sin\theta\cos\theta}{M_B^2 - s} \\ \dfrac{-\cos\theta\sin\theta}{M_A^2 - s} + \dfrac{\sin\theta\cos\theta}{M_B^2 - s} & \dfrac{\sin^2\theta}{M_A^2 - s} + \dfrac{\cos^2\theta}{M_B^2 - s} \end{vmatrix} ,$$

$$\cos^2\theta = \frac{1}{2} + \frac{1}{2}\frac{(1/2)(M_1^2 - M_2^2)}{\sqrt{(1/4)(M_1^2 - M_2^2)^2 + B_{12}B_{21}}} . \quad (4.6)$$

The states $|A\rangle$ and $|B\rangle$ are the superpositions of the initial levels, $|1\rangle$ and $|2\rangle$, as follows:

$$|A\rangle = \cos\theta|1\rangle - \sin\theta|2\rangle , \qquad |B\rangle = \sin\theta|1\rangle + \cos\theta|2\rangle . \quad (4.7)$$

Generally, the representation of the states $|A\rangle$ and $|B\rangle$ as superpositions of initial states is valid when one cannot neglect the s-dependence of functions $B_{ij}(s)$ and their imaginary parts are not small. Let us consider the propagator matrix near $s = M_A^2$:

$$\hat{D} = \frac{1}{\Pi(s)} \begin{vmatrix} M_2^2(s) - s & B_{12}(s) \\ B_{21}(s) & M_1^2(s) - s \end{vmatrix} \simeq \frac{-1}{\Pi'(M_A^2)(M_A^2 - s)} \begin{vmatrix} M_2^2(M_A^2) - M_A^2 & B_{12}(M_A^2) \\ B_{21}(M_A^2) & M_1^2(M_A^2) - M_A^2 \end{vmatrix} . \quad (4.8)$$

In the left-hand side of Eqn (4.8), the singular (pole) terms are the only surviving ones. The matrix determinant in the right-hand side of Eqn (4.8) is equal to zero:

$$\left[M_2^2(M_A^2) - M_A^2\right]\left[M_1^2(M_A^2) - M_A^2\right] - B_{12}(M_A^2)B_{21}(M_A^2) = 0 . \quad (4.9)$$

This equality follows from Eqn (4.4) which fixes $\Pi(M_A^2) = 0$. It allows us to introduce the complex mixing angle:

$$|A\rangle = \cos\theta_A|1\rangle - \sin\theta_A|2\rangle . \quad (4.10)$$

The right-hand side of Eqn (4.8) can be re-written, using the mixing angle θ_A, as follows:

$$\left[\hat{D}\right]_{s\sim M_A^2} = \frac{N_A}{M_A^2 - s} \begin{vmatrix} \cos^2\theta_A & -\cos\theta_A\sin\theta_A \\ -\sin\theta_A\cos\theta_A & \sin^2\theta_A \end{vmatrix} , \quad (4.11)$$

where

$$N_A = \frac{1}{\Pi'(M_A^2)}\left[2M_A^2 - M_1^2 - M_2^2\right] ,$$

$$\cos^2\theta_{\rm A} = \frac{M_{\rm A}^2 - M_2^2}{2M_{\rm A}^2 - M_1^2 - M_2^2}\,,$$

$$\sin^2\theta_{\rm A} = \frac{M_{\rm A}^2 - M_1^2}{2M_{\rm A}^2 - M_1^2 - M_2^2}\,. \qquad (4.12)$$

We recall that in Eqn (4.12) the functions $M_1^2(s)$, $M_2^2(s)$ and $B_{12}(s)$ are fixed at the point $s = M_{\rm A}^2$. In the case under consideration, when the angle $\theta_{\rm A}$ is a complex magnitude, the values $\cos^2\theta_{\rm A}$ and $\sin^2\theta_{\rm A}$ do not determine the probabilities of states $|1\rangle$ and $|2\rangle$ in $|A\rangle$; indeed, the values $\sqrt{N_{\rm A}}\cos\theta_{\rm A}$ and $-\sqrt{N_{\rm A}}\sin\theta_{\rm A}$ are the transition amplitudes $|A\rangle \to |1\rangle$ and $|A\rangle \to |2\rangle$. Therefore, the corresponding probabilities are equal to $|\cos\theta_{\rm A}|^2$ and $|\sin\theta_{\rm A}|^2$.

In order to analyse the content of the state $|B\rangle$, an analogous expansion of the propagator matrix should be made near the point $s = M_{\rm B}^2$. After introducing

$$|B\rangle = \sin\theta_{\rm B}|1\rangle + \cos\theta_{\rm B}|2\rangle\,, \qquad (4.13)$$

we have the following expression for $\hat{D}$ in the vicinity of the second pole $s = M_{\rm B}^2$:

$$\left[\hat{D}\right]_{s\sim M_{\rm B}^2} = \frac{N_{\rm B}}{M_{\rm B}^2 - s}\begin{vmatrix} \sin^2\theta_{\rm B} & \cos\theta_{\rm B}\sin\theta_{\rm B} \\ \sin\theta_{\rm B}\cos\theta_{\rm B} & \cos^2\theta_{\rm B}\end{vmatrix}, \qquad (4.14)$$

where

$$N_{\rm B} = \frac{1}{\Pi'(M_{\rm B}^2)}\left[2M_{\rm B}^2 - M_1^2 - M_2^2\right],$$

$$\cos^2\theta_{\rm B} = \frac{M_{\rm B}^2 - M_1^2}{2M_{\rm B}^2 - M_1^2 - M_2^2}\,,$$

$$\sin^2\theta_{\rm B} = \frac{M_{\rm B}^2 - M_2^2}{2M_{\rm B}^2 - M_1^2 - M_2^2}\,. \qquad (4.15)$$

In Eqn (4.15) the functions $M_1^2(s)$, $M_2^2(s)$ and $B_{12}(s)$ are fixed at the point $s = M_{\rm B}^2$.

If B_{12} depends weakly on s and one can neglect this dependence, the angles $\theta_{\rm A}$ and $\theta_{\rm B}$ coincide. But generally they are different. So the formulae for the propagator matrix differ from the standard approach of quantum mechanics by this very point.

Another distinction is related to the type of the level shift afforded by the mixing; namely, in quantum mechanics the levels 'repel' each other from the mean value $1/2(E_1 + E_2)$ [see also Eqn (4.5)]. Generally, Eqn (4.4) can cause the 'repulsion' of squared masses from the mean value, $1/2(M_1^2 + M_2^2)$, as well as their 'attraction'.

The scattering amplitude for the one-channel case is defined by the following expression:

$$A(s) = g_i(s)D_{ij}(s)g_j(s)\,. \qquad (4.16)$$

In the multichannel case, $B_{ij}(s)$ is a sum of loop diagrams:

$$B_{ij}(s) = \sum_n B_{ij}^{(n)}(s)\,, \qquad (4.17)$$

where $B_{ij}^{(n)}$ is the loop diagram in the channel n, $g_i^{(n)}$, the $g_j^{(n)}$ being vertex functions and ρ_n the phase space factor. The partial scattering amplitude in channel n is:

$$A_n(s) = g_i^{(n)}(s)D_{ij}(s)g_j^{(n)}(s)\,. \qquad (4.18)$$

4.2 The overlapping of a large number of resonances: construction of the propagator matrix

Let us consider the propagator matrix $\hat{D}$ for an arbitrary number of resonances. The matrix elements D_{ij} describe the transition from the input state i [with propagator $(m_i^2 - s)^{-1}$] to the state j. They obey a system of linear equations as follows:

$$D_{ij} = D_{ik}B_{kj}(s)(m_j^2 - s)^{-1} + \delta_{ij}(m_j^2 - s)^{-1}\,, \qquad (4.19)$$

where $B_{ij}(s)$ is the loop diagram for the transition and δ_{ij} is the Kronecker symbol. Let us introduce the diagonal propagator matrix $\hat{d}$ for input states :

$$\hat{d} = \mathrm{diag}\left((m_1^2 - s)^{-1}, (m_2^2 - s)^{-1}, (m_3^2 - s)^{-1}, \ldots\right). \qquad (4.20)$$

Then the system of linear equations (4.19) can be re-written in a matrix form, as follows:

$$\hat{D} = \hat{D}\hat{B}\hat{d} + \hat{d}\,. \qquad (4.21)$$

We obtain

$$\hat{D} = \frac{I}{(\hat{d}^{-1} - \hat{B})}\,. \qquad (4.22)$$

The matrix $\hat{d}^{-1}$ is diagonal, thus $\hat{D}^{-1} = (\hat{d}^{-1} - \hat{B})$ is of the form:

$$\hat{D}^{-1} = \begin{vmatrix} M_1^2 - s & -B_{12}(s) & -B_{13}(s) & \ldots \\ -B_{21}(s) & M_2^2 - s & -B_{23}(s) & \ldots \\ -B_{31}(s) & -B_{32}(s) & M_3^2 - s & \ldots \\ \vdots & \vdots & \vdots & \vdots \end{vmatrix}, \qquad (4.23)$$

where M_i^2 is defined by Eqn (4.3). After inversion of this matrix, we obtain a full set of elements $D_{ij}(s)$:

$$D_{ij}(s) = \frac{(-1)^{i+j}\Pi_{ji}^{(N-1)}(s)}{\Pi^{(N)}(s)}\,. \qquad (4.24)$$

Here $\Pi^{(N)}(s)$ is the determinant of the matrix $\hat{D}^{-1}$ and $\Pi_{ji}^{(N-1)}(s)$ is a matrix supplement to the element $[\hat{D}^{-1}]_{ji}$, i.e. the determinant of matrix $\hat{D}^{-1}$ with the jth line and ith column excluded.

The zeros of $\Pi^{(N)}(s)$ define the poles of the propagator matrix which correspond to physical resonances formed by the mixing. We denote the complex masses of the resonances as

$$s = M_{\rm A}^2,\ M_{\rm B}^2,\ M_{\rm C}^2, \ldots \qquad (4.25)$$

Near the point $s = M_{\rm A}^2$, one can keep only the leading pole term in the propagator matrix. This means that the free term in Eqn (4.21) can be neglected, so we get a system of homogeneous equations:

$$D_{ik}(s)\left(\hat{d}^{-1} - \hat{B}\right)_{kj} = 0\,. \qquad (4.26)$$

The solution of this system defined up to the normalization factor does not depend on the initial index i. Then the elements of the propagator matrix may be written in a factorized form as follows:

$$\left[\hat{D}^{(N)}\right]_{s\sim M_{\rm A}^2} = \frac{N_{\rm A}}{M_{\rm A}^2 - s}\cdot\begin{vmatrix} \alpha_1^2, & \alpha_1\alpha_2, & \alpha_1\alpha_3, & \ldots \\ \alpha_2\alpha_1, & \alpha_2^2, & \alpha_2\alpha_3, & \ldots \\ \alpha_3\alpha_1, & \alpha_3\alpha_2, & \alpha_3^2, & \ldots \\ \ldots & \ldots & \ldots & \ldots \end{vmatrix}, \qquad (4.27)$$

where N_A is the normalization factor and the complex coupling constants obey the equation:

$$\alpha_1^2 + \alpha_2^2 + \alpha_3^2 + \ldots + \alpha_N^2 = 1\,. \tag{4.28}$$

The constants α_i are the normalized amplitudes for the transition *resonance* A $\to$ *state i*. The probability of finding state *i* in a physical resonance A is

$$w_i = |\alpha_i|^2\,. \tag{4.29}$$

An analogous representation of the propagator matrix can also be made in the vicinity of other poles:

$$D_{ij}^{(N)}(s \sim M_B^2) = N_B\,\frac{\beta_i\beta_j}{M_B^2 - s}\,,$$

$$D_{ij}^{(N)}(s \sim M_C^2) = N_C\,\frac{\gamma_i\gamma_j}{M_C^2 - s}\,,\ \ldots \tag{4.30}$$

The coupling constants satisfy normalization conditions similar to Eqn (4.28):

$$\beta_1^2 + \beta_2^2 + \ldots + \beta_N^2 = 1\,, \qquad \gamma_1^2 + \gamma_2^2 + \ldots + \gamma_N^2 = 1\,, \ldots \tag{4.31}$$

However, generally there is no completeness condition for the inverse expansion:

$$\alpha_i^2 + \beta_i^2 + \gamma_i^2 + \ldots \neq 1\,. \tag{4.32}$$

For two resonances, this means that $\cos^2\Theta_A + \sin^2\Theta_B \neq 1$. Still, let us recall that the equality in the inverse expansion, which is relevant to the completeness condition, appears in the models where the *s*-dependence of loop diagrams is neglected [see Eqns (4.5) – (4.7)].

4.3 Full resonance overlapping: the accumulation by one resonance of the widths of its neighbors

Let us consider two examples which describe the idealized situation of a full overlapping of two or three resonances. In these examples, the effect of the accumulation by one resonance of the widths of its neighbors can be seen in its primary intact form.

(a) A full overlapping of two resonances.

For the sake of simplicity, let B_{ij} be a weak *s*-dependent function, so Eqn (4.5) can be used. We define:

$$M_1^2 = M_R^2 - \mathrm{i}M_R\Gamma_1\,, \qquad M_2^2 = M_R^2 - \mathrm{i}M_R\Gamma_2\,, \tag{4.33}$$

and

$$\mathrm{Re}\,B_{12}(M_R^2) = P\int_{(\mu_1+\mu_2)^2}^{\infty}\frac{\mathrm{d}s'}{\pi}\,\frac{g_1(s')g_2(s')\rho(s')}{s' - M_R^2} \to 0\,. \tag{4.34}$$

It is possible that $\mathrm{Re}\,B_{12}(M_R^2)$ can be zero at positive g_1 and g_2, provided the contribution from the integration region $s' < M_R^2$ cancels the contribution from the region $s' > M_R^2$. In this case

$$B_{12}(M_R^2) \to \mathrm{i}g_1(M_R^2)g_2(M_R^2)\rho(M_R^2) = \mathrm{i}M_R\sqrt{\Gamma_1\Gamma_2}\,. \tag{4.35}$$

After substituting Eqns (4.33) – (4.35) into Eqn (4.5), one has

$$M_A^2 \to M_R^2 - \mathrm{i}M_R(\Gamma_1 + \Gamma_2)\,, \qquad M_B^2 \to M_R^2\,. \tag{4.36}$$

Therefore, after the mixing, one of the states accumulates the widths of the primary resonances, $\Gamma_A \to \Gamma_1 + \Gamma_2$, and the other state becomes a quasi-stable particle, with $\Gamma_B \to 0$.

(b) A full overlapping of three resonances.

Consider the equation

$$\Pi^{(3)}(s) = 0 \tag{4.37}$$

in the same approximation as in the above example. Correspondingly, we put

$$\mathrm{Re}\,B_{ab}(M_R^2) \to 0 \quad (a \neq b)\,;$$

$$M_i^2 = M_R^2 - s - \mathrm{i}M_R\Gamma_i = x - \mathrm{i}\gamma_i\,. \tag{4.38}$$

A new variable, $x = M_R^2 - s$, is used and we denote $M_R\Gamma_i = \gamma_i$. Taking account of $B_{ij}B_{ji} = -\gamma_i\gamma_j$ and $B_{12}B_{23}B_{31} = -\mathrm{i}\gamma_1\gamma_2\gamma_3$, we can re-write Eqn (4.37) as follows:

$$x^3 + x^2(\mathrm{i}\gamma_1 + \mathrm{i}\gamma_2 + \mathrm{i}\gamma_3) = 0\,. \tag{4.39}$$

Therefore, at full overlapping of the resonances, one obtains

$$M_A^2 \to M_R^2 - \mathrm{i}M_R(\Gamma_1 + \Gamma_2 + \Gamma_3)\,,$$

$$M_B^2 \to M_R^2\,, \qquad M_C^2 \to M_R^2\,. \tag{4.40}$$

Resonance A accumulates the widths of three primary resonances, and the states B and C become quasi-stable and degenerate.

4.4 The resonances $f_0(1300)$, $f_0(1500)$, $f_0(1530^{+90}_{-250})$, and $f_0(1780)$

The *K*-matrix analysis provides a basis for the investigation of the mixing phenomenon in the scalar sector. The propagator matrix technique used in the next stage of the analysis allows us to restore correctly the contribution from the real parts of the loop diagrams, $B_{ij}(s)$, thus having correctly calculated the contribution of input states to the formation of physical resonances.

The resonance mixing in the region 1200 – 1600 MeV may be considered in the two-channel approximation, for the quark – hadron duality justifies the use of the quark channels $n\bar{n}$ and $s\bar{s}$. Correspondingly,

$$B_{ij}(s) = \cos\varphi_i\cos\varphi_j B_{ij}^{(n\bar{n})}(s) + \sin\varphi_i\sin\varphi_j B_{ij}^{(s\bar{s})}(s)\,, \tag{4.41}$$

where i, j run over $1, 2, 3, 4$ with the following notation for the states: $1 = {}^3\mathrm{P}_0(n\bar{n}\ \textit{rich})$, $2 = {}^3\mathrm{P}_0(n\bar{n}\ \textit{rich})$, $3 = \textit{gluonium}$, and $4 = 2^3\mathrm{P}_0(s\bar{s}\ \textit{rich})$. The quark states are usually described with light-cone variables. Then

$$B_{ij}^{(n\bar{n})}(s) = \frac{1}{(2\pi)^3}\int_0^1\frac{\mathrm{d}x}{x}\int \mathrm{d}^2k_\perp\,\frac{g_i(s')g_j(s')}{s' - s}\,2(s' - 4m^2)\,. \tag{4.42}$$

Here $s' = (m^2 + k_\perp^2)/x(1-x)$ and m is the non-strange quark mass. The factor $2(s' - 4m^2)$ is due to the quark spin variables:

$$\mathrm{Tr}\left[(\hat{k} + m)(-\hat{p} + \hat{k} + m)\right] = 2(s' - 4m^2)\,.$$

An analogous expression, with the replacement $m \to m_s$, defines $B_{ij}^{(s\bar{s})}(s)$.

The simplest parametrization of the vertex function for the transition from input state i in quarks is:

$$g_i(s) = \gamma_i \sqrt[4]{s} \left[\frac{k_i^2 + \sigma_i}{k^2 + \sigma_i} - d_i \frac{k_i^2 + \sigma_i}{k^2 + \sigma_i + h} \right]. \quad (4.43)$$

Here $k^2 = s/4 - m^2$ and $k_a^2 = m_a^2/4 - m^2$, where m is the constituent quark mass equal to 350 MeV for a non-strange quark and 500 MeV for strange one, and m_a is the mass of the input state.

For the first state, $1^3P_0(n\bar{n}\ rich)$, and for the gluonium we put $d_1 = d_3 = 0$. The second state is radial excitation, 2^3P_0, and its wave function is orthogonal to that of the ground state. This means that the real part of the function $B_{12}(s)$ must tend to zero at s close to resonance masses. Such an orthogonalization was performed at the point $\sqrt{s} = 1.5$ GeV, thus determining the value of the coefficient d_2. The vertex functions for the same nonet members are equal, so $g_2(s) = g_4(s)$.

The parameters m_a, γ_a, h and σ_a are defined by the masses and widths of physical resonances. However, the mass m_a can be approximately fixed by the K-matrix pole: $\mu_a^2 \simeq m_a^2 - \mathrm{Re}\, B_{aa}(\mu_a^2)$. It should be underlined that m_3 is the mass of a pure gluonium, which is a subject of lattice QCD.

The positions of the amplitude poles and the masses of input states found in Ref. [7] by fitting the 0^{++} wave are shown in Table 4. The relative weight of a primary state in the physical resonance A is defined by Eqn (4.29); calculated in such a way that the probabilities W_a for the resonances under investigation are shown in Table 4.

Table 4. Masses and mixing angles of the input states, the content of physical states and the positions of poles for the 0^{++} amplitude (masses in GeV).

Solution I				
Probability of resonance	$1^3P_0(n\bar{n}\ rich)$ $\phi_1 = 18^\circ$ $m_1 = 1.457$	$2^3P_0(n\bar{n}\ rich)$ $\phi_2 = -6^\circ$ $m_2 = 1.536$	Gluonium $\phi_3 = 25^\circ$ $m_3 = 1.230$	$2^3P_0(s\bar{s}\ rich)$ $\phi_4 = 84^\circ$ $m_4 = 1.750$
$W[f_0(1300)]$ $1.300 - i0.115$	32%	12%	55%	1%
$W[f_0(1500)]$ $1.500 - i0.065$	25%	70%	3%	2%
$W[f_0(1530)]$ $1.450 - i0.450$	44%	24%	27%	4%
$W[f_0(1780)]$ $1.780 - i0.085$	1%	1%	0%	98%
Solution II				
Probability of resonance	$1^3P_0(n\bar{n}\ rich)$ $\phi_1 = 18^\circ$ $m_1 = 1.107$	$2^3P_0(n\bar{n}\ rich)$ $\phi_2 = 35^\circ$ $m_2 = 1.566$	Gluonium $\phi_3 = 25^\circ$ $m_3 = 1.633$	$2^3P_0(s\bar{s}\ rich)$ $\phi_4 = -55^\circ$ $m_4 = 1.702$
$W[f_0(1300)]$ $1.300 - i0.115$	35%	26%	38%	0.4%
$W[f_0(1500)]$ $1.500 - i0.065$	1%	64%	35%	0.4%
$W[f_0(1530)]$ $1.450 - i0.450$	12%	41%	47%	0.3%
$W[f_0(1780)]$ $1.750 - i0.100$	0.1%	0.2%	0.2%	99.5%

As was stressed above, in order to make comparisons with the QCD calculations, one should separate contributions from large and small distances, that is, take into account the short-range interaction component, $r < r_0 \sim R_{\mathrm{confinement}}$, and eliminate the contribution from large r. Therefore, in the calculation of masses, which might be compared with the results of QCD-motivated models, we should make a replacement in the amplitude of the 0^{++} wave, as follows:

$$B_{ab}(s) \to \mathrm{Re}\, \bar{B}_{ab}(s, k_0^2) = P \int_{4m^2+4k_0^2}^{\infty} \frac{\mathrm{d}s'}{\pi} \frac{g_a(s')\rho(s')g_b(s')}{s' - s} 2(s' - 4m^2). \quad (4.44)$$

The poles of the amplitude re-determined in this way provide the masses which are related to the interaction at $r < 1/k_0$. One must compare the masses obtained with a cutting of the order of $k_0^2 \sim 0.125$ (GeV s^{-1})^2, that corresponds to accounting for the quark interaction at $r \leqslant 1\ fm \sim R_{\mathrm{confinement}}$ with the quark model results.

For Solution I we get (the values are given in GeV)

	$1^3P_0(s\bar{s}\ rich)$	$1^3P_0(n\bar{n}\ rich)$	$2^3P_0(n\bar{n}\ rich)$	$2^3P_0(s\bar{s}\ rich)$
$m(k_0^2 = 0) = \mu_a^{\mathrm{bare}}$	0.720	1.360	1.577	1.791
$m(k_0^2 = 0.125)$	0.730	1.340	1.560	1.780
$m(k_0^2 \to \infty) = m_a$	—	1.457	1.536	1.750.

(4.45)

For Solution II:

	$1^3P_0(s\bar{s}\ rich)$	$1^3P_0(n\bar{n}\ rich)$	$2^3P_0(n\bar{n}\ rich)$	$2^3P_0(s\bar{s}\ rich)$
$m(k_0^2 = 0) = \mu_a^{\mathrm{bare}}$	0.720	1.357	1.585	1.734
$m(k_0^2 = 0.125)$	0.735	1.340	1.570	1.725
$m(k_0^2 \to \infty) = m_a$	—	1.107	1.566	1.702.

(4.46)

In Refs [6, 7] the lightest $q\bar{q}$ state, $f_0^{\mathrm{bare}}(720)$, has not been included in the mixing machinery. In Eqns (4.45) and (4.46) the mass corrections for this state have been evaluated to be $m_a(k_0^2) \simeq m_a^2 - \mathrm{Re}\, \bar{B}_{aa}(m_a^2, k_0^2)$. This approximate equality is due to the comparative smallness of the non-diagonal loop diagram contributions.

Results (4.45) and (4.46) prove that the values m_a ($k_0^2 = 0.125$ GeV^2) slightly differ from μ_a^{bare}, while the differences from the input masses m_a can be significant. This means that the K-matrix analysis provides approximately correct meson characteristics, which may be compared with the quark model results. On the contrary, one should compare the values of the input masses, m_a, which can differ noticeably both from the masses of bare states, μ_a^{bare}, and from the masses of real resonances, with the results of lattice QCD.

4.5 Dynamics of glueball mixing with the $q\bar{q}$ states

To discover the glueball mixing with the $q\bar{q}$ states, let us make a replacement in the loop diagrams of the propagator matrix:

$$g_a(s) \to \xi g_a(s), \quad (4.47)$$

with the factor ξ changing in the interval $0 \leqslant \xi \leqslant 1$. At $\xi = 0$ the mixing is switched off, and the amplitude has poles at $s = m_a^2$. Figure 15 demonstrates the position of the poles at different ξ for Solutions I and II. With increasing ξ, the poles move from the real axis to the lower part of the complex plane. Let us discuss in detail the dynamics of the pole movement for Solution II.

At $\xi = 0.1 - 0.5$ the glueball state of Solution II is mainly mixed with the state $2^3P_0(n\bar{n})$, while at $\xi = 0.8 - 1.0$ the mixing with the state $1^3P_0(n\bar{n}\ rich)$ becomes important. As a result, the state which is the glueball descendant, sunk rather

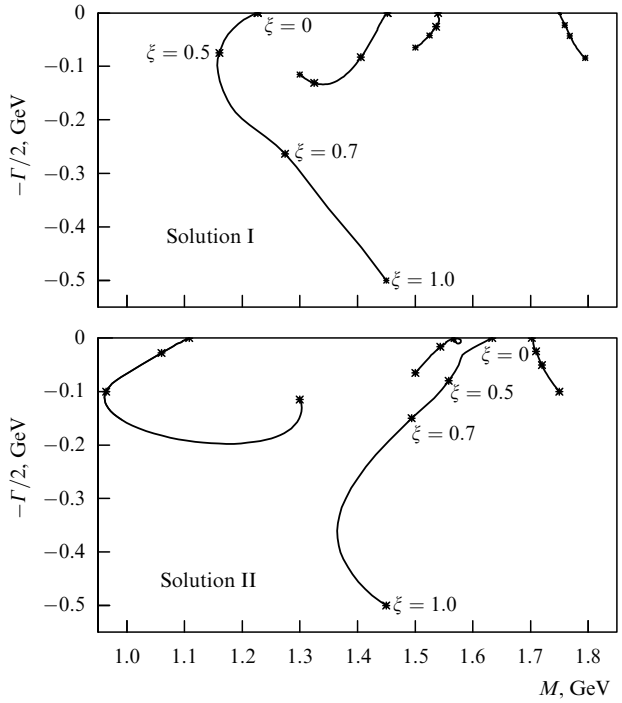

Figure 15. Variation of the resonance pole positions plotted on the complex M-plane for different coupling constants $g_a \to \xi g_a$.

deeply into the complex plane, acquires a mass $M = 1450 - i450$ MeV, and the glueball component of this broad resonance is 47%. Likewise, in Solution I the broad resonance is a glueball descendant as well.

The hypothesis about strong mixing of the gluonium with $q\bar{q}$ states had been raised formerly. But attempts of quantitative reconstruction of the picture of mixing within the standard quantum mechanics approach failed, for two phenomena were lost:

(1) The $q\bar{q}$-glueball mixing described by the D matrix can lead not only to the repulsion of levels, that follows from the standard quantum mechanical approach, but to their attraction as well. The latest effect is caused by the presence of the imaginary part in the loop diagram B_{ab}, and it is important that Im B_{ab} is not small near 1500 MeV.

(2) Resonance overlapping leads to the repulsion of poles located on the imaginary axis of masses, and one resonance accumulates the widths of the others.

Just this kind of mixing happened at 1500 MeV, and the large width of one of the resonances is the inevitable consequence. It is also natural that the broad resonance itself is the gluonium descendant, for the gluonium mixes, without any significant suppression, with the nearby $q\bar{q}$ states, both of them being dominantly non-strange ones.

5. Conclusions

The deconfinement of quarks from the excited $q\bar{q}$ levels goes in two stages:

(1) The unavoidable production of $q\bar{q}$ pairs, which form two or more white states (hadrons).

(2) The flying away of the produced hadrons, their interaction and, as a result, the mixing of neighboring $q\bar{q}$ levels, that leads to the formation of a broad locking state, which plays the role of a dynamical barrier for neighboring levels.

This is the K-matrix analysis, together with the dispersion N/D method, which are summoned to decipher the second stage of the deconfinement. The analysis of the 00^{++} wave carried out in the K-matrix or the propagator matrix techniques demonstrated that the lightest scalar glueball, being near the states $1^3P_0q\bar{q}$ and $2^3P_0q\bar{q}$, after mixing turned into a broad state, with $\Gamma/2 \simeq 500$ MeV. This broad state $f_0(1530^{+90}_{-250})$ carries about half of the scalar gluonium component, whereas the other components of the broad resonance are $1^3P_0q\bar{q}$ and $2^3P_0q\bar{q}$.

It looks like the waves 00^{-+} and 02^{++} behave similarly [57], which allows us to believe that the future of the physics of highly excited states is tightly related to the study of broad states both in the search for exotic hadrons and the investigation of confinement phenomenon.

Acknowledgements. It is with pleasure that I express my deep gratitude to L G Dakhno and V A Nikonov for help. This research is supported by RFBR grant No. 96-02-17934 and the INTAS – RFBR grant No. 95-0267.

References

1. Fritzsch H, Gell-Mann M, in *Proc. of the XVI Int. Conf. on High Energy Phys., Batavia* **2** 135 (1972); Fritzsch H, Minkowski P *Nuovo Cimento A* **30** 393 (1975); Freund P G O, Nambu Y *Phys. Rev. Lett.* **34** 1645 (1975)
2. Jaffe R L, Johnson K *Phys. Lett. B* **60** 201 (1976)
3. Bali G S et al. *Phys. Lett. B* **309** 378 (1993)
4. Sexton J, Vaccarino A, Weingarten D *Phys. Rev. Lett.* **75** 4563 (1995)
5. Morningstar C, Peardon M "Efficient glueball simulations on anisotropic lattices" hep-lat/9704011; *Phys. Rev.* **56** 4043 (1997)†
6. Anisovich A V, Anisovich V V, Prokoshkin Yu D, Sarantsev A V *Z. Phys. A* **357** 123 (1997)
7. Anisovich A V, Anisovich V V, Sarantsev A V *Phys. Lett. B* **395** 123 (1997); *Z. Phys. A* **359** 173 (1997)
8. t'Hooft G *Nucl. Phys. B* **72** 461 (1974); Veneziano G *Nucl. Phys. B* **117** 519 (1976)
9. Particle Data Group: Barnett R M et al. *Phys. Rev. D* **54** 1 (1996)
10. Heusch C A "Gluonium — an unfulfilled promise of QCD?", in *QCD–20 Years Later* (Eds P M Zerwas, H A Kastrup) (Singapore: World Scientific, 1993)
11. Savinov V (CLEO Collab.) "A measurement of the form factors of light pseudoscalar mesons at a large momentum transfer" hep-ex/9507005, *Proc. of the 10th Int. Workshop on Photon–Photon Collisions, Sheffield, UK, 1995* (Singapore: World Scientific, 1995) p. 203; Behrend H J et al. (CELLO Collab.) *Z. Phys. C* **49** 401 (1991); Aihara H et al. (TCP/2γ Collab.) *Phys. Rev. Lett.* **64** 172 (1990)
12. Anisovich V V, Melikhov D I, Nikonov V A *Phys. Rev. D* **55** 2918 (1997); Anisovich V V et al. *Phys. Lett. B* **404** 166 (1997)
13. Anisovich V V *Usp. Fiz. Nauk* **165** 1225 (1995) [*Phys. Usp.* **38** 1179 (1995)]
14. Anisovich V V et al. *Phys. Lett. B* **355** 363 (1995)
15. Aker E et al. (Crystal Barrel Collab.) *Phys. Lett. B* **260** 249 (1991)
16. Anisovich V V et al., in *Proc. of Second Biennial Workshop on Nucleon-Antinucleon Physics* (*NAN'93*) (Moscow, 1993); Anisovich V V et al. *Yad. Fiz.* **57** 1666 (1994) [*Phys. Atom. Nucl.* **57** 1595 (1994)]
17. Anisovich V V et al. *Phys. Rev. D* **50** 1972 (1994)
18. Anisovich V V et al. (Crystal Barrel Collab.) *Phys. Lett. B* **323** 233 (1994)
19. Amsler C et al. (Crystal Barrel Collab.) *Phys. Lett. B* **333** 277 (1994)
20. Amsler C, Close F E *Phys. Rev. D* **53** 295 (1996); *Phys. Lett. B* **353** 385 (1995)
21. Close F E, Farrar G R, Li Z "Determining the gluonic content of isoscalar mesons" hep-ph/9610280; *Phys. Rev. D* **55** 5749 (1997)
22. Weingarten D "Scalar quarkonium and scalar glueball" hep-lat/9608070; *Nucl. Phys. B, Proc. Suppl.* **63** 232 (1998)

† See, for example, http://xxx.lanl.gov.

23. Genovese M "A unified picture of glueball candidates $f_0(1500)$ and $f_0(1700)$" hep-ph/9608451; *Phys. Rev. D* (to be published)
24. Alde D et al. *Z. Phys. C* **66** 375 (1995); Prokoshkin Yu D, Kondrashov A A, Sadovskiĭ S A *Dokl. Akad. Nauk* **342** 473 (1995) [*Phys. Dokl.* **40** 266 (1995)]
25. Binon F et al. *Nuovo Cimento A* **78** 313 (1983)
26. Binon F et al. *Nuovo Cimento A* **80** 363 (1984)
27. Hyams B et al. *Nucl. Phys. B* **64** 134 (1973)
28. Lindenbaum S J, Longacre R S *Phys. Lett. B* **274** 492 (1992); Etkin A et al. *Phys. Rev. D* **25** 1786 (1982)
29. Anisovich V V, Sarantsev A V *Phys. Lett. B* **382** 429 (1996)
30. Anisovich V V, Prokoshkin Yu D, Sarantsev A V *Phys. Lett.* **389** 388 (1996)
31. Alston-Garnjost M et al. *Phys. Lett. B* **36** 152 (1971)
32. Anisovich V V et al. *Phys. Rev. D* **42** 3045 (1990)
33. Peters K, Klempt E *Phys. Lett. B* **352** 467 (1995)
34. Anisovich V V *Phys. Lett. B* **364** 195 (1995)
35. Zou B S, private communication (1996)
36. Anisovich V V, Prokoshkin Yu D, Kondashov A A, Sadovsky S A, Sarantsev A V "The two-pion spectra for the reaction $\pi^- p \to \pi^0\pi^0 n$ at 38 GeV/c pion momentum and combined analysis of the GAMS, Crystal Barrel and BNL data" hep-ph/9711319
37. Aston D et al. *Nucl. Phys. B* **296** 493 (1988)
38. Weinstein J, Isgur N *Phys. Rev. Lett.* **48** 659 (1982); *Phys. Rev. D* **27** 588 (1983); **41** 2236 (1990); Lohse D et al. *Nucl. Phys. A* **516** 513 (1990); Janssen G et al. *Phys. Rev. D* **52** 2690 (1995)
39. Jaffe R J *Phys. Rev. D* **15** 267 (1977); Achasov N N, Shestakov G N *Z. Phys. C* **41** 309 (1988)
40. Ritter C et al. *Phys. Lett. B* **380** 431 (1996)
41. Close F E et al. *Phys. Lett. B* **319** 291 (1993)
42. Anisovich A V, Sarantsev A V "*K*-matrix analysis of the $K\pi$ S-wave in the mass region 900–2100 MeV and nonet classification of the scalar $q\bar{q}$ states" hep-ph/9705401, *Phys. Lett. B* **413** 137 (1997)
43. Chew G F, Mandelstam S *Phys. Rev.* **119** 467 (1960)
44. Anisovich V V et al. *Nucl. Phys. A* **544** 747 (1992); Anisovich V V et al. *Nucl. Phys. A* **563** 549 (1993)
45. Anisovich A V, Sarantsev A V *Yad. Fiz.* **55** 2163 (1992) [*Sov. J. Nucl. Phys.* **55** 1200 (1992)]; Anisovich A V, Sadovnikova V A *Yad. Fiz.* **55** 2657 (1992) [*Sov. J. Nucl. Phys.* **55** 1483 (1992)]
46. Kapitanov A V, Sarantsev A V *Yad. Fiz.* **56** 156 (1993) [*Phys. Atom. Nucl.* **56** 89 (1993)]
47. Anisovich V V, Shekhter V M *Nucl. Phys. B* **55** 455 (1973); Bjorken J D, Farrar G R *Phys. Rev. D* **9** 1449 (1974)
48. Voloshin S A, Nikitin Yu P, Porfirov P I *Yad. Fiz.* **35** 1006 (1982) [*Sov. J. Nucl. Phys.* **35** 586 (1982)]
49. Gershtein S S, Likhoded A K, Prokoshkin Yu D *Z. Phys. C* **24** 305 (1984)
50. Anisovich A V "Three-body dispersion – relation N/D equations for the coupled decay channels $p\bar{p} \to \pi\pi\pi, \eta\pi\pi, K\bar{K}\pi$" hep-ph/9610523; Anisovich A V *Yad. Fiz.* **58** 1467 (1995) [*Phys. Atom. Nucl.* **58** 1383 (1995)]; Anisovich A V, Leutwyler H *Phys. Lett. B* **375** 335 (1996)
51. Zou B S, Bugg D V *Phys. Rev. D* **50** 591 (1994); Morgan D, Pennington M R *Phys. Rev. D* **48** 1185 (1993)
52. Flatté S M *Phys. Lett. B* **63** 224 (1976)
53. Kondashov A A et al., in *Proc. 27th Int. Conf. on High Energy Phys.* (Glasgow, 1994) p. 1407; Kondrashov A A et al., Preprint IHEP 95-137 (Protvino: IHEP, 1995)
54. Zheng Z *The XVI Int. Symp. on Lepton and Photon Interactions, Ithaca, New York, 1993* (Eds P Drell, D Rubin), in *AIP Conf. Proc.* **302** 530 (1994)
55. Amsler C et al. *Phys. Lett. B* **342** 433 (1995); Amsler C et al. (Crystal Barrel Collab.) **355** 425 (1995)
56. Bugg D V et al. *Phys. Rev. D* **50** 4412 (1994); Bugg D V, Sarantsev A V, Zou B S *Nucl.Phys. B* **471** 59 (1996)
57. Bugg D V, private communication (1997)